QATAR UNIVERSITY

COLLEGE OF ARTS AND SCIENCES

THERMAL STABILIZATION AND MECHANICAL PROPERTIES OF NANOCRYSTALLINE AL AND AL-LI ALLOYS

BY

SARA IYAD AHMAD

A Thesis Submitted to the Faculty of

the College of Arts & Sciences

in Partial Fulfillment

of the Requirements

for the Degree of

Master of Science in

Materials Science & Technology

June, 2016

COMMITTEE PAGE

The members of the Committee approve the thesis of Sara Iyad Ahmad defended

on 26th of May 2016.

Dr. Khaled Youssef
Thesis/Dissertation Supervisor

Dr. Ahmed Ayesh
Committee Member

Dr. Ahmed Abdalla
Committee Member

Approved:

Dr. Eiman Mustafawi, Dean, College of Arts & Sciences

ABSTRACT

Aluminum alloys in the conventional grain size state have had their share of research and are implemented in a variety of applications in our everyday life such as being the main structural materials in automobiles, aircrafts, solar panels supports and stations. Hence, it is long overdue to design light-weight aluminum alloys for the best performance in their nanostructured state. However, the strength associated with the reduced grain size of nanomaterials is associated with a penalty that leads to microstructural instabilities that result in grain growth, limiting their service temperatures and expected lifetime. Two mechanisms have been suggested to suppress grain growth: The first is a thermodynamic approach concerned with reducing the overall free energy of the system by lowering the grain boundary energy through solute segregation, and the second is kinetically by reducing grain boundary mobility.

In this thesis, nanocrystalline (nc) Al and Al-2 at.% Li alloy are synthesized by mechanical cryomilling. It is proved that adding 1 at.% strontium (Sr) thermally stabilized the nc Al and its alloy up to 873 K, which represents 94% of its homologous temperature along with maintaining its exceptionally high hardness and good ductility, resulting in an alloy that has a specific strength higher than that of steel. Mechanical properties and thermal stability were studied through several characterization techniques such as XRD, TEM, micro-hardness, sheer punch tests, and SEM. It is concluded that thermal stabilization has occurred through both thermodynamic and kinetic mechanisms. Hence we anticipate that the results of this research will highly motivate the development

of thermally stabilized, super-light and ultra-tough nanostructured materials for technological and structural applications.

Table of Contents

List of Tables

List of Figures

Acknowledgements

I would like to express my great appreciation to those whom without their continuous support and encouragement, this work wouldn't have been accomplished in its final form.

Above all, I would like to express my deepest gratitude to my research supervisor Dr. Khaled Youssef, for introducing me to this field of research, for sharing with me his exceptional knowledge and experience, to never failing to answer any of my questions, and for guiding me throughout the entire course of this research journey. His dedication to his work and the wide knowledge he possesses are the kind of characters I aim for as a scientist.

My great appreciation goes to my committee members Dr. Ahmed Ayesh and Dr. Ahmed Abdalla for their time, and for their valuable comments and useful suggestions that helped in guiding the development of this research work. Assistance provided by the staff of the Center of Advanced Materials (CAM) and the Central Lab Unit (CLU) throughout the experimental work of this research is highly appreciated.

Special gratitude is given to Prof. Mariam Al-Maadeed for giving me the opportunity to join the Materials Science and Technology program as a student and a graduate assistant, for giving me the opportunity to participate in many conferences to expand my knowledge and share my work, and for her continuous support and encouragement.

Finally, this work wouldn't have been possible without the support of the special people in my personal life, my family.

Dedication

To my entire family, for your encouragement, your support, and for putting up with my demanding schedule throughout this journey. To my incredible parents, my role model and the driving force behind the pursue of my education. To my husband Issa, for your patience, encouragement, help, and understanding, without which this work wouldn't have been completed.

Chapter 1. Introduction

Nanocrystalline materials (nc) are simply conventional materials which have been reduced in size to reach less than 100 nm. The reason behind the attention this class of materials gained in research studies is their exceptional mechanical properties that overcome those of their conventional coarse-grained counterparts. Even after several decades, the research community is still pursuing the understanding of the relationships between their processing, structure, and properties [1].

The significant mechanical properties of this class of materials rise from their unique microstructure. This uniqueness stems from the high density of grain boundaries and the grain boundary structure, leading to changes in their physical, mechanical, as well as chemical properties [2]. A better understanding of the grain boundary structure and its effect on the mechanical properties of nc materials is given in section 2.1.

Two of the widely studied mechanical properties are strength/hardness and ductility. Significant values of hardness and strength have been observed and reported for a variety of materials and alloys. However, up till recently, it seemed that the increase in strength is at the expense of a reduced ductility. Improvements in processing techniques and characterization methods have helped in achieving more promising results and is leading towards a better understanding of ductile behavior in nc materials [1], [2]. Examples from literature on the achieved hardness and ductility for different nc materials can be found in section 2.2.

One of the first relationships achieved between the grain size of materials and their hardness and strength was the Hall-Petch relationship which was named after the two scientists that independently reached the same conclusion. That is, the reduction of grain size of materials results in an increase in their strength and hardness [3]. This effect is further discussed in section 2.2.

One of the issues that were noted over time was the different experimental findings obtained for the same materials, sometimes even prepared by the same laboratory. The research community became aware that the nc structure as well as properties depend significantly on the synthesis route. Hence choosing the appropriate synthesis technique is one of the first steps towards attaining the desired results [4]. Synthesis processes of nc materials are classified under two categories: bottom-up and top-down [2]. The differences between these two categories are highlighted in section 2.3.

For this work, mechanical alloying which belongs to the top-down techniques is the synthesis process of choice to synthesize nc Al and Al-2 at.% Li alloy for reasons made apparent in section 2.3. The main principle behind the reduction in grain size in this technique is the accumulation of structural defects produced by the repeated wilding and fracturing of the powders as a result of the continuous collision between the milling media and the powders. As a result, high density of dislocations is introduced which eventually make up the grain boundaries of the new smaller grains [5].

Unfortunately, the exceptional mechanical properties that are attainable by the reduction of the grain size of materials and metals to the nano range are associated with a penalty

that leads to microstructural instabilities. This is due to the structure of the new introduced grain boundaries which leads to the increase in the overall energy of the system. As a result, the material is termed unstable and the grains tend to grow back to their conventional size losing their nanostructures and the exceptional properties that came along [6].

Despite the driving force for grains to grow, substantial stabilization against grain growth has been reported for several nc materials. However, all materials reported to have achieved thermal stabilization are either alloys or materials that contained impurities. As a result, two strategies have been developed to suppress grain growth in nc materials and achieve thermal stability, either thermodynamically or kinetically, but with the crucial involvement of solute atoms [7]. The effect of solute atoms on both strategies and examples of thermal stability achieved by both mechanisms are reported in details in section 2.4.

1.1 Significance & Novelty

Conventional grained lithium-containing aluminum alloys have had their extensive share in research worldwide. Reduced density, enhanced specific strength and high stiffness-to-weight ratio are among the advantages such alloys can offer over other commercial aluminum alloys. Hence their significance in weight-critical structures whether for military, space, structural or everyday applications cannot be neglected [8]. It is long overdue to design aluminum-lithium based alloys for the best performance in their nanostructured state, where the expected increase in strength along with their light weight

promise to achieve a specific strength that is higher than that of steel. Production of lightweight nanomaterials with improved strength, ductility and other superior properties is an important step towards improving fuel economy and reducing greenhouse gas emissions, not to mention its effect and influence on structural applications.

Within the past decades, the processing of Al and its alloys has been under extensive studies [9]–[11]. Yet literature lacks the research about nc Al-Li alloys. This is due to the many challenges that have been encountered by researches to reduce the grain size of Al due to its high ductility, and to maintain its thermal stability at high temperatures due to grain growth.

The innovation of this thesis is to overcome these two challenges and produce thermally stable nc Al and Al-Li alloys. This is done through synthesizing Al and Al-Li via a mechanical cryomilling process along with dilute additions of carefully selected non-equilibrium solutes to produce non-equilibrium solid solution powders. This will lead to grain boundary segregation of the dopant during annealing to thermally stabilize the nano materials. Accordingly, we propose novel alloy development via powder processing to fabricate nc lightweight, thermally stable Al, and Al-Li based alloys with ultra-high strength and hardness, and good ductility.

Hence, conducting this research does not only guide other future research possibilities on other Al alloys, but is also considered a stepping stone in the direction to enhancing structural functions and technologies to be applied around the world.

1.2 Objective & Hypothesis

The objective of this thesis is to study the effect of adding dilute amount of strontium (Sr) as solute atoms on the thermal stability of the grain boundaries and hence the grain size and mechanical properties of nc Al and aluminum-lithium based alloys (Al-2 at.% Li).

Hence the hypothesis of this thesis is the following:

Adding small concentrations of Sr, as much as 1 at.%, to nc Al and Al-2 at.% Li nano-alloy will thermally stabilize the grain structure and inhibit grain growth by segregating to the grain boundaries and reducing the grain boundary energy in order to maintain their exceptional mechanical properties.

Chapter 2. Literature Review

2.1. Nanocrystalline Materials

Tailoring the properties of materials to satisfy the required applications is dependent upon the control of their grain size [12]. Nanocrystalline (nc) materials, defined as those with a grain size less than 100 nm [1], have proven to attain exceptional mechanical properties that exceed those of coarse-grained and alloyed metals of which the grain size is greater than 1μm [1], [2], [9], [13]–[16]. The growing interest in the mechanical behavior of this class of materials originated from the remarkable predictions that were first made by the pioneers of this field and the first to prepare nc materials, Gleiter and his co-workers, that nc metals must show an increase in their ductility and a substantial increase in both hardness and strength of a factor that is according to them, can be as high as 10 or more times higher, compared to their conventional grain size materials with the same chemical composition [13], [17]. As a result, nc metals are leading their way to be recognized as the new class of high performance engineering materials to be used for various technological and structural applications.

Materials in this class can be categorized based on their dimensionality starting with (1) 0D nanoparticles or nanoclusters, (2) 1D multi-layered nanostructure, (3) 2D nanograined layers or filamentary, and (4) 3D equiaxed bulk solids [18]. Discussion in this thesis will be limited to the main interest which is equiaxed nc or 3D bulk solid metals.

The distinctive atomic structure of this class of materials is the main source of the excellent mechanical properties such materials can exhibit. This structural uniqueness stems from the presence of the high density of intercrystalline components such as grain boundaries, which can represent up to 50% of the entire crystal volume. As a result, the deformation of these materials is highly affected by grain boundaries resulting in a significant alteration to their physical, mechanical, and chemical properties considerably compared to their coarse-grained counterparts [13]. Due to this high density of interfaces or grain boundaries in nc materials, as the grain size is further decreased, the number of atoms that lay in the grain boundary regions or will exist near the interfaces increase [19]. In addition, the atoms in those regions are highly disordered, due to their high volume fraction. A schematic representation of the difference in the arrangement of atoms at perfect crystal sites and at grain boundaries is shown in Figure 2.1.

The schematic representation assumes a cross section of a hard-sphere model of a nc material with the grain-boundary atoms (open circles) are clearly not defined with any crystalline symmetry, in contrary to the crystal atoms (closed circles) [13].

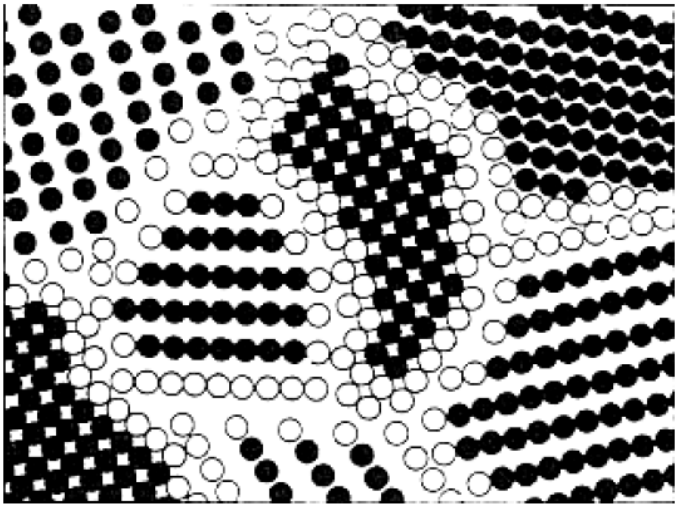

Figure 2. 1 Schematic representation of the arrangement of atoms in perfect crystal sites and in grain boundaries through a hard-sphere model of a nc material [13]

Experimental investigations using transmission electron microscopy (TEM) confirms the previously explained grain boundary structure. Figure 2.2 shows TEM micrographs of nc electrodeposited Ni and nc Cu prepared by gas phase condensation. It can be clearly concluded that crystallinity continues throughout the grain and up until the grain boundary of the nc metals [1].

A variety of reviews had been conducted to summarize the pioneering ideas and concepts behind nc materials after Gleiter's original predictions by Gleiter [20], Weertman [21], Kumar et al. [1], Koch [22] Meyers et al. [2].

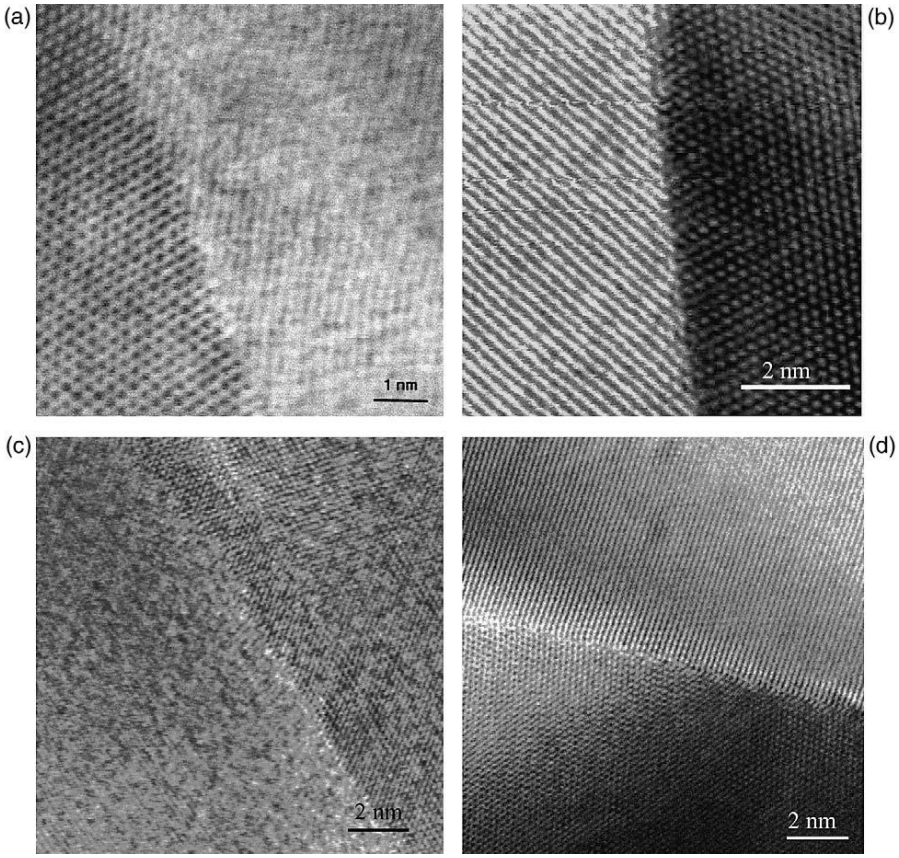

Figure 2. 2. High resolution TEM micrographs of showing the lack of crystallinity in the grain boundaries of (a,b) electrodeposited nc-Ni, and (c,d) nc-Cu produced by gas-phase condensation [1]

2.2. Mechanical Properties of Nanocrystalline Materials

Over the past few decades, tailoring microstructures using grain refinement tools to design enhanced materials properties had and is still having the attention of metallurgical research [1]. However, the research field became aware of the fact that using different synthesis methods to produce nc metals leads to variations in the final product and the resultant mechanical properties. Such variations include dislocation densities, impurity

contents and flaw content to name a few [2], [4], resulting in different experimental findings which sometimes were not due to the intrinsic material behavior, but rather to the difficulties encountered with synthesizing full-density and artifact-free samples [1]. Nonetheless, several advances have been made in the field of synthesizing nanoscale particles and bulk nanostructured materials, in addition to the rise in sophistication of characterization tools, led to the attainment of more accurate results [1], [2].

Even though proving some of the previously mentioned predictions of mechanical properties such as high strength and hardness was never an issue, experimental results of other properties such as ductility, which was predicted to increase as the grain size decreased, had not been realized easily and is still a topic of interest for ongoing research [16]. However, advancement in research especially in processing nc metals and their characterization methods resulted in synthesizing limited cases of nc structures with high yield and ultimate tensile strengths along with good ductility [9], [14], [15], [23]–[25].

2.2.1 Hardness and Strength of Nanocrystalline Materials

The fact that ultrahigh strength and high hardness can be achieved in nc metals is the main reason for the continuous attraction towards this class of materials. Research had been conducted over the past decades for several nc metals synthesized with different techniques to prove that their enhanced hardness as a result of nanocrystallinity. Examples include nc electroplated nickel [26], gas-condensed palladium, copper [27], and mechanically milled zinc [28].

More recent studies have been able to achieve more significant results. Youssef et al. [15] synthesized nc Cu spheres using a novel in-situ consolidation technique with an average grain size of 23 nm. A significant tensile strength of 1120 MPa that is 11 times higher than that of conventional micro-sized Cu was reported. In addition, it exhibited yield strength of 791 MPa, the highest amongst earlier reported yield strength for nc Cu in tensile tests [29], [30]. These high strength values and the high hardness of 2.3 GPa were attributed to the nanocrystallinity of the synthesized spheres [15]. Figure 2.3 shows a comparison between this in-situ consolidated copper, and other nc Cu prepared by inert gas condensation [31].

Botcharova et al. [32] synthesized a nc Cu–10 at.% Nb alloy with a grain size less than 50 nm by mechanical alloying followed by powder consolidation. The authors attributed the mechanical strength of 1.6 GPa obtained from the Cu–10 at.% Nb alloy to the grain boundary hardening mechanism referring to the Hall–Petch relation due to the fact that no inverse Hall-Petch behavior was observed.

Youssef et al. [9] used the same in situ consolidation technique used in [15] to produce a 26 nm Al-5083 or Al-Mg alloy. As shown in Figure 2.4 curve C, the alloy reached exceptionally high tensile yield strength that is four times higher than that of conventional micro-size grained Al-5083 (Figure 2.4 curve A) and a maximum tensile strength of 620 MPa and 740 MPa, respectively. Authors concluded the strengthening mechanism to be a result of strain hardening due to grain refinement and the accumulation of dislocations during plastic deformation. A similar strength was achieved

in the same alloy produced by Han et al. [33] through cryomilling followed by cold isotactic pressing (CIP) consolidation. However as seen in Figure 2.4 curve D, the alloy had negligible % elongation unlike the alloy represented by curve C. This is attributed to the synthesis process itself and the large amounts of impurities introduced into the material during milling which increased the brittleness of the alloy.

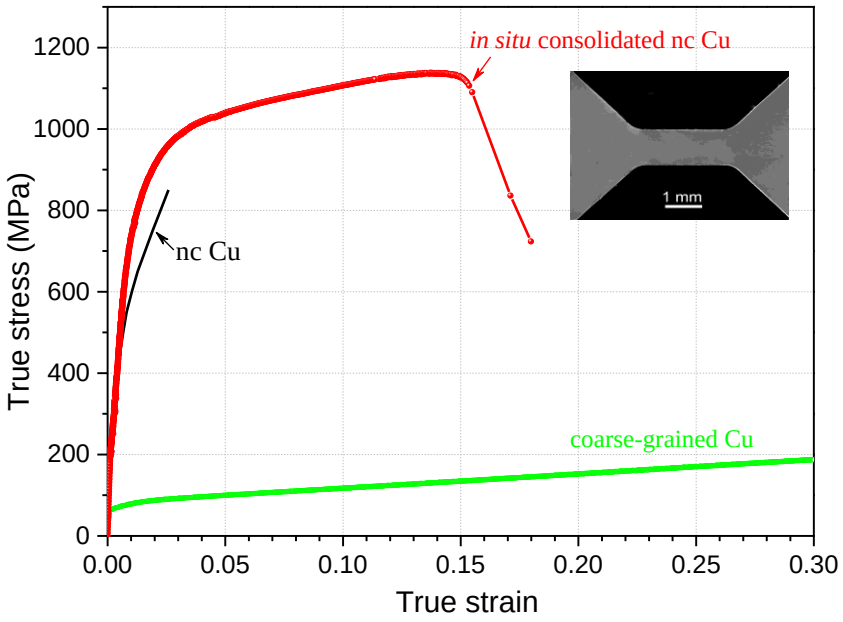

Figure 2. 3. A comparison of the mechanical behavior of the bulk in-situ consolidated nc Cu [15], coarse grained Cu (grain size > 80 mm), and nc Cu prepared by inert gas condensation and compaction [31] via a typical tensile stress-strain curve.

Sasaki et al. [34] produced Al-5 at.% Fe by mechanical alloying followed by plasma sintering. Structural analysis of the bulk alloy revealed that it is a bimodal system consisting of some coarse α-Al grains and other nc α-Al and Al_6Fe grains. A high compressive yield strength value of 1 GPa was reported and attributed to the nano structured α-Al and Al_6Fe phases. By the end of this section, it becomes evident that a significant increase in strength and hardness can be achieved in materials that are produced with a nanogarin size.

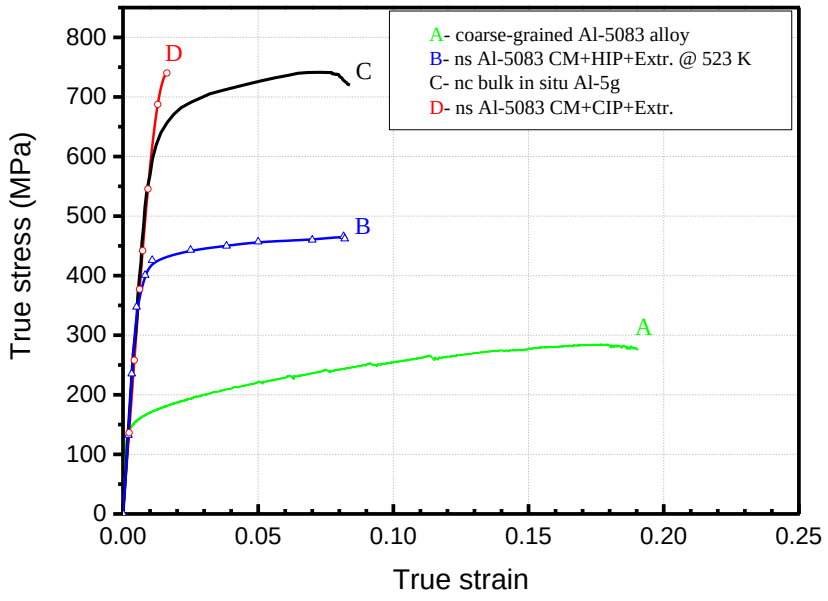

Figure 2. 4. A comparison of the mechanical behavior of the bulk in-situ consolidated nc Al-5%Mg (C) [9], coarse grained Al-5083 (A) (grain size > 55 µm), cryomilled and HIP consolidated at 523 K ns Al-5083 (B) [39], & cryomilled and CIP consolidated nc Al-5083 (30nm) (D) [33].

2.2.2 Ductility of Nanocrystalline Materials

While it has never been an issue to realize high strength and hardness in nc metals, one of the main obstacles was and is still to sustain any amount of uniform elongation or in other words to achieve any amount of considerable ductility alongside those ultra-high strength properties [35]–[37]. Hence in this section, the light is shed on some examples of nc metals that demonstrated poor ductility, along with some recent studies that showed significant improvements. In general, reducing the grain size of metals in the conventional region results in an increase in ductility, however, the ductility in the nano regime is so low for metals that when in the conventional grain size, they exhibit tensile ductility elongation of 40-60% [35]. Figure 2.5 shows the trend of reduction in ductility with increasing strength for some nc metals [22].

This behavior of limited ductility was mainly attributed to either artifacts that result from processing nanomaterials such as porosity, or to the deformation mechanisms in the nano regime that are not fully understood yet such as lack of strain hardening causing the mechanical instability of nc metals [35].

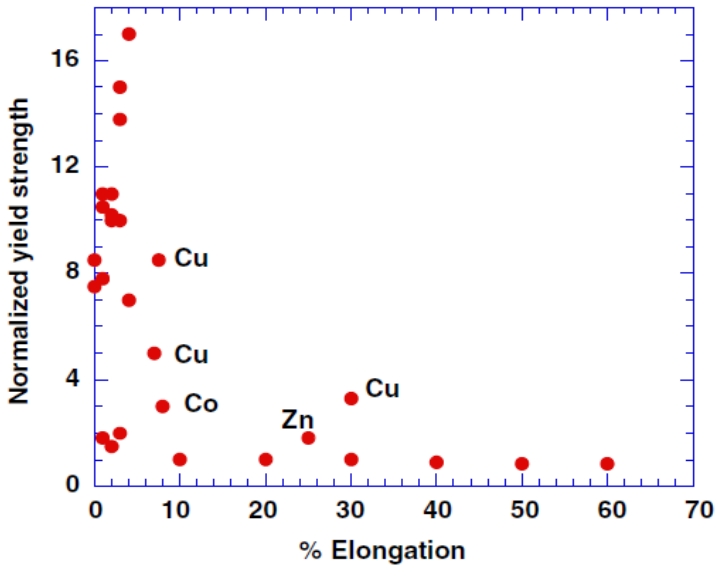

Figure 2. 5. Normalized yield strength vs. % elongation in tension of nc metals showing the trend of reduction in ductility with increasing strength [22].

A bimodal grain size distribution was suggested as a method for attaining an increase in ductility [30]. Zhang et al. [38] synthesized nc Zn by cryomilling for 4 hours to exhibit a combination of high strength and good ductility. Studying the microstructure of this sample revealed a 30% volume fraction and a combination of small nc grains and grains larger than 50 nm. This suggested that the obtained strength was a result of the presence of the nc smaller grains, while the larger grains provided the dislocation activity along with strain hardening which gave rise to the exhibited improved ductility.

Tellkamp synthesized a bimodal Al based alloy (Al-5083) which showed a combination of high strength and good ductility and is shown in Figure 2.4 as curve B. The alloy was produced by cryomilling and consolidation by hot isotactic pressing (HIP) and reported to

achieve a ductility elongation of 8.4% and 462 tensile strength [39]. However, comparing curve B with curve C, the curve for the 26 nm nc Al-5083 alloy prepared by in-situ consolidation mentioned in the previous section which has also achieved a similar total elongation of 8.5% [9], it is clearly seen that the increase in ductility for the bimodal alloy is achieved at the expense of a lower strength, where curve C achieved a combination of a much higher 740 MPa ultimate tensile strength.

Looking back at Figure 2.3, which shows the true stress-strain behavior of the 23 nm Cu spheres that were mentioned in the previous section and synthesized by Youssef et al. [15] with a tensile strength of 1120 MPa and yield strength of 791 MPa, the metal exhibited 14% and 15.5% uniform elongation and elongation to failure, respectively. A ductility behavior that has never been reported for any other nc Cu which usually exhibits a low ductility of 2% [29], [30], [40].

The justification for this improved ductility was captured by the bright field TEM BFTEM micrographs shown in Figure 2.6. In previous studies, strain hardening which is the dominant plastic deformation mode of ductile coarse-grained materials caused by the normal dislocation activity, was believed to be suppressed in nc grains due to the theoretical predictions of the impossibility of dislocation pile-ups in nano-grains [41], [42]. However in this study, the BFTEM micrographs taken for a 23 nm single grain showed that it exhibited a significant number of dislocations which piled up (Figure 2.6 a) and increased as the applied strain increased (Figure 2.6 c). Furthermore, the

dislocation pile-ups still existed in the grain even after further straining initiated a crack leading to the grain failure (Figure 2.6 d) [15].

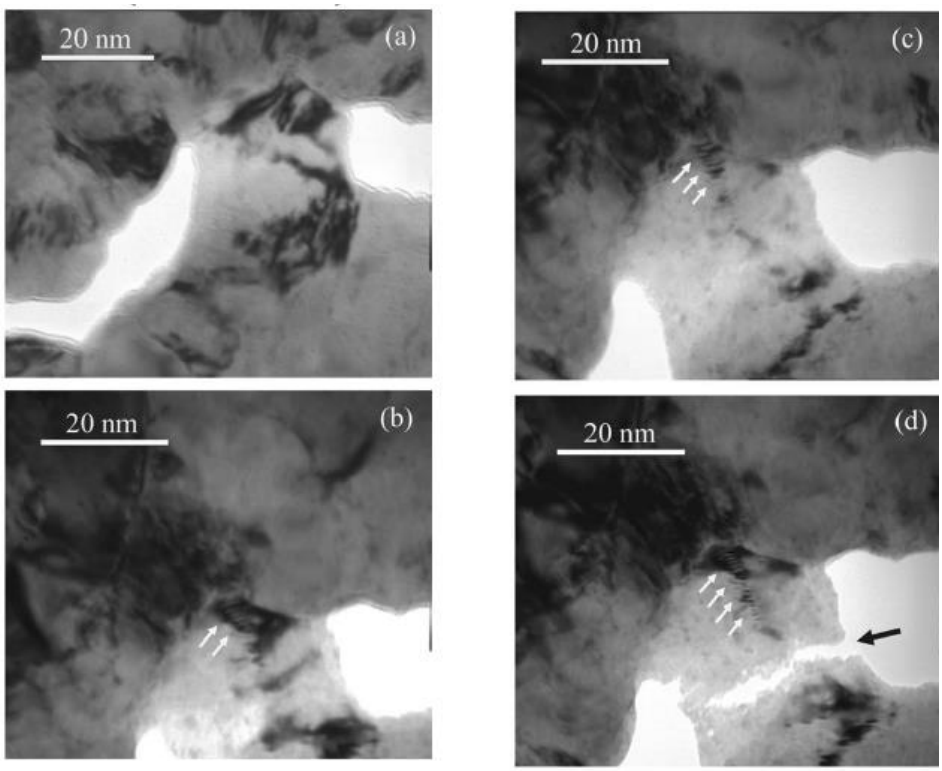

Figure 2. 6. Bright field TEM micrographs of a 23 nm Cu grain showing the dislocation activity and dislocation pile-ups with increasing strain even after crack is initiated [15]

It is believed that defects, such as porosity, that are introduced to nano materials during processing are responsible for the ductility limitations in this class of materials. Hence, a combination of high strength and good ductility can be achieved as a result of

synthesizing artifact-free bulk nc materials [9], [15], [23], [24]. The formation mechanism of these artifact-free nc metals prepared in these cases by in-situ consolidation, and hence the improved ductility, are not fully understood yet. Still, the experimental observations of the presence of lattice dislocations suggest strain hardening to be the major deformation mechanism. In addition, it is suggested that cryomilling which is milling at liquid nitrogen temperature allows for the formation of those dislocation pile-ups and high dislocation densities, which in addition allows for the nanoscale grain sizes to be achieved in shorter times, resulting in minimizing contamination during milling [9], [15].

Even though the combination of ultrahigh strength and improved ductility of nc metals has only been observed in a limited number of cases, it opens doors of research opportunities and shows great technological and structural promises in making what was impossible in the past possible today.

2.2.3 Hall-Petch Relation

The aim of this section is to answer the question why should nc metals attain enhanced mechanical properties compared to their counter parts, especially strength and hardness. Colin Humphreys succeeded to simplify all is what to be explained in the following sections by a simple quote: “Crystals are like people, it is the defects in them which tend to make them interesting!” [43]. Hence, understanding the defects, imperfections, or impurities that lay in the structure of such class of materials is the key to understanding

their behavior. The main defects of interest for this discussion are dislocations and grain boundaries.

It was as early as the 18th century when it was noted and reported that the finer the grains, the better the properties of iron, and the higher the quality of steel. Nonetheless, it was not until a series of groundbreaking observations and papers had been published in the 1950's that such relationship was proved. In such papers, the observation of dislocations had been made and hence had proven to exist by the use of the electron microscope. In addition, the independent research conducted and published by E.O.Hall and N.J.Petch had led them to attain the same conclusions between grain boundary and strength [44].

As a result, the key relationship [3] was named after both scientists, to be known the Hall-Petch relationship, and is defined by the following equation:

$$\sigma_y = \sigma_o + kd^{-1/2} \qquad \text{eq.2.1}$$

Where σ_y is the yield stress, σ_o is a material constant and is the resistance of the lattice to dislocation motion, k is also a material constant, and d is the average grain size or grain diameter. As the equation suggests the yield stress and as a consequence the strength of materials is expected to increases as the grain size of material decrease. The main mechanism responsible for this behavior is the dislocation pileups at the grain boundaries. This phenomenon is referred to as grain-boundary strengthening and as its

name suggests, it can be explained by understanding the structure of grain boundaries and its effect on dislocation motion.

Grain boundaries are considered as barriers to dislocation motion which leads to pinning further dislocation propagation for two main reasons, disorientation and disorder. Extra energy is required to change the dislocation direction to cross from one grain to the other due to the crystallographic disorientation of adjacent grains. In addition, the atoms inside grain boundaries are highly disordered, making it difficult for the dislocations to peruse from one grain to another in a continuous manner. With continued applied stress, dislocations keep propagating to the grain boundary and cause additional pile up. Each dislocation is associated with its own repulsive stress field, and those repulsive forces combine with the applied stress to overcome the grain boundary diffusion barrier [45], [46].

As logic suggests, as the grain size gets smaller, less dislocations can pile up within the grain, the lower the repulsive forces applied by those dislocations and the higher the applied stress that is necessary to allow for dislocation to propagate and cause deformation. This results in a higher yield strength of the material [12], [47]. Thus, resulting in a justification for the inverse relationship between grain size and the yield strength such as described by the Hall–Petch equation.

Even though it is now well known and experimentally proven that reducing the grain size of metals is the main reason for its enhanced strength and hardness, a controversy that lingers in the field of nanomaterials is the extent of validity of the Hall-petch relation. In

other words, whether it applies over all ranges of grain sizes of nanomaterials, or is there a critical grain size beyond which this relationship is no longer valid.

On one hand, several studies reported a continuous increase in hardness with decreasing grain size for different metals. Gas condensed nc palladium and copper [25], [48], [49], ball-milled nc iron [50], nc Ni [51] and nc Ni-W [52] are among those studies where the tested nc samples exhibited a Hall-Petch dependence down to the smallest grain size tested.

On the other hand, other research had doubted the expected high strength for nc materials as a decrease in the yield stresses and hence the strength was reported below a critical grain size [1], [53], [54]. In an attempt to understand this behavior, a great deal of effort has been carried and varied are the models that have been proposed to explain the deformation mechanism in nc materials [2], [12], [55], [56]. However the experimental support for those proposed models is notably sparse and the breakdown of the Hall-Petch equation is a controversial topic.

One of the main earlier justifications for this so-called behavior was simply the possibility of accommodating dislocation pile-ups in such small sized grains [12], [47]. Yet as was noted earlier, dislocation activity was recorded in TEM images in a number of cases [15], [57], [58], proving the existence of this deformation activity in materials in the nano-range.

Another modest justification arose from the variation in the strength data reported for the same material such as Cu, where it would follow the Hall-Petch effect to grain sizes as small as 10 nm in some studies [25], [59], or it would exhibit the inverse Hall-Petch effect in others [60]. As a result, it became clear that such effect can be simply attributed to the imperfections in the sample material such as defects, flaws, porosity or contamination [55], [60].

Another simple reasoning had been realized from the Hall-Petch behavior observed in pure Ni and Ni–P alloy, where the relationship is maintained down to the amorphous limit [52]. In other words, the amorphous state is the lower limit of the nc state, after which a breakdown in the relationship seems logical as crystallinity is no longer maintained, and the strength decreases with further decrease in grain size [2].

2.3 Synthesis of Nanostructured Metals and Alloys

A clear effort has been made by researchers and several are the techniques that have been developed over the years to produce nc materials. All those techniques fall under two main categories which are the bottom-up and top-down approaches. Bottom-up method means building the nanostructure by assembling it atom-by-atom and layer-by-layer as in consolidating small clusters. The most common methods under this category are inert gas condensation and electrodeposition. In the top-down approach, a nanostructured material is obtained by simply breaking down the structure of a bulk polycrystalline material into a nanometer sized crystallites. The two most commonly used techniques under this

category are mechanical milling, and other severe plastic deformation techniques such as equal channel angular pressing (ECAP) and high pressure torsion [2].

A discussion of all the synthesis techniques is beyond the scope of this work. Hence, the discussion will be limited to high energy ball-milling as it is the chosen method for the synthesis of nc materials in this thesis, for the reasons and advantages that will be highlighted in the coming sections.

2.3.1 High Energy Ball Milling

Mechanical milling or ball milling is a top down synthesis technique used to produce materials with nanostructures by disintegrating the coarse grained structure of those materials' elemental powders [2], [61]. The process is referred to by mechanical alloying when the starting powder mixture contains two or more materials to be milled together. As a result, material transfer occurs during milling and the product is a nanoalloy [61]. Another type of milling is called cryomilling where the milling process is carried out at very low temperatures such as cryogenic temperatures or in a cryogenic media such as liquid nitrogen [61]. This method is of great importance for ductile and soft materials, especially FCC structures such as aluminum alloys [1]. The use of liquid nitrogen is to embrittle those materials to prevent the problem of softening and welding during milling, as it tends to cause the produced material to be bigger in size than the powders' original size [1].

In mechanical milling, the selected powder materials are put in a steel vial along with the milling media, which consists of a number of steel balls of certain sizes. The vial is then

sealed to prevent oxidation in an inert atmosphere of high purity argon. The main principle behind the reduction in grain size in this technique is the accumulation of structural defects produced by the repeated mechanical deformation of the powders, as a result of the high energy rotation of the milling balls inside the vial, represented in Figure 2.7 A. This leads to the collision of the balls which leads to crushing the powders trapped in between, just as represented in Figure 2.7 B, with high impact force into nanocrystallites [2], [61].

The deformation mechanisms by which the structural changes occur can be divided into a three steps process. The first step is the local deformation in shear bands that contain a high density of dislocations. With continued deformation, dislocation density increase and dislocations start to annihilate and rearrange forming new grain boundaries for the new nanograins, which represents the second step. In the third step, the nanostructure is extended throughout the sample with continued milling and the grains are randomly oriented and separated by high-angle grain boundaries [5].

The minimum obtainable grain size depends on the competition between the deformation processes of the material and its thermal recovery [4], [61]. Mechanical milling has been used in a wide range of research to synthesize nanocrsytalline metals and their alloys such as Al [11], [62], [63], Cu [64]–[66], Ni [67], [68], Fe [69], [70], Mg [71], [72], and many other metals [5].

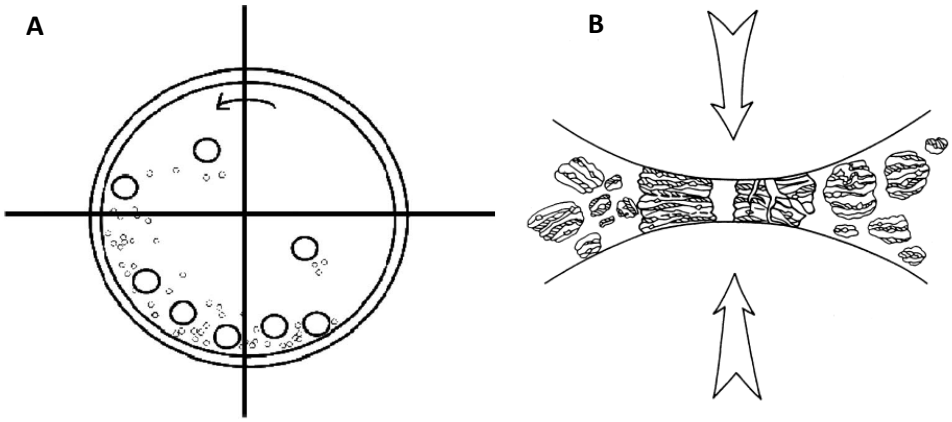

Figure 2. 7. Schematic representations of the rotation of material inside the milling vial (A) and the crushing of materials as a result of balls collisions (B) [2]

2.3.2 Advantages of Mechanical Alloying

Many are the advantages for mechanical alloying that made it the technique of choice to be used in the preparation of our nc Al and Al alloys. These advantages start with the production of powder particles and the production of smallest possible grain size [61], [73]. This is true even for ductile materials such as FCC structured metals or metals with low melting points, as cryomilling can be used to embrittle such materials and produce powder particles [74].

In addition, as most of the other synthesis techniques have shown a small capacity of production, high-energy mechanical alloying has shown capability to produce large quantities of nanomaterials up to several kilograms per day [2]. Another very important

advantage of this technique is its ability to produce novel alloys that cannot be synthesized by any other technique. An example of that would be synthesizing alloys from immiscible elements which otherwise do not attain an equilibrium room temperature solubility. Hence, this technique is known as a non-equilibrium technique as a result of its capability to increase the solid solubility limit beyond the conventional limit and create super saturated solid solutions. This is due to the large segregation sites as a result of the large grain boundary density in nc materials [61], [74], [75].

In addition, this can be attributed to two main factors that are of crucial importance in the nanostructured state, the large change in elastic enthalpy and large negative enthalpy of mixing. In conventional states, systems which exhibit the first factor have a minimum solid solubility, whilst in nanostructured materials the diffusion of those insoluble solutes from the solid solution to the grain boundaries is a prerequisite for reducing the high grain boundary energy. Once diffusion is accomplished and grain boundary energy is reduced, the second factor is important for resisting the formation of a secondary phase [74].

One disadvantage that may be associated with mechanical milling is the possibility of contaminating the milled samples by impurities from the milling vessel, milling media or milling atmosphere [1]. Hence it is advised that chemical analysis is conducted after milling to check for the level of impurities in the sample, if any.

2.4. Thermal Stabilization

Unfortunately, the exceptional mechanical properties that are attainable by the simple reduction of the grain size of materials and metals to the nano range eventually diminish back to their original values. This is due to the lack of thermal stability of such materials at temperatures that are as low as room temperature. As a result, grains tend to grow back to their conventional size losing their nanostructures and the exceptional properties that came along.

This thermal instability is referred to as grain growth and is of crucial importance for technological and scientific reasons. The technological aspect refers to the synthesis and processing of such materials where most synthesis methods produce nc in a powder form before consolidating it into bulk. The consolidation process often requires the use of heat or pressure, which can easily initiate grain growth [7].

While from a scientific point of view, understanding grain growth is the first step towards developing strategies to prevent it. This should be done by investigating the stability of not only the microstructure of the grains of such materials but as well as the structure of their grain boundaries, as they are the reason behind this thermal instability [7].

2.4.1 Grain Growth

The reason behind the ultrahigh strength of this class of materials is mainly grain refinement, as in this mechanism, reducing grain size means introducing more grain boundaries that act as barriers to intra-grain dislocation motion resulting in a material that

is harder to deform. However, the strength associated with the new reduced grain size is associated with a penalty that leads to microstructural instabilities. This is due to the high volume fraction of grain boundaries which will lead the atoms to occupy unfavorable interfacial positions energetic wise [7], [76]. Hence, the increase in the overall free energy of the system can be directly related to the structure of the grain boundaries in nc materials [74], [76].

It follows that the atomic system will tend to pursue stabilization by seeking an atomic configuration that shall allow for the lowest energy possible. As a result, the atomic system tends to eliminate the root of the problem which is the large number of grain boundaries and solve the problem by grain growth. Thus the removal of grain boundaries becomes the driving force to decreasing the system's energy [65] as can be understood from the change in the Gibbs free energy, G, with respect to the change in grain boundary area, A, and its proportionality with the grain boundary energy, γ [76].

$$dG \propto \gamma dA \qquad \text{eq.2.2}$$

Grain growth can be represented as an expansion of a curved interface with the driving force or pressure (P) is given by [77]:

$$P = \alpha \frac{\gamma}{r} \qquad \text{eq.2.3}$$

Where α is a constant, γ is the free energy of the grain boundary per unit area, and r is the radius of the grain. As seen from equation 2.3, the smaller the grain size, the higher the

pressure or the driving force for grain growth, and this pressure can be as large as 1 GPa when r is as small as tens of nanometers.

Grain growth have been reviewed by many researchers [6] and nc metals such as Ni, Cu, Al, Pb, Pd, Mg, and Zn have been reported to undergo grain growth at low temperatures staring from room temperature [76], [78]. Figure 2.8 shows the trend of grain growth vs. the reduced annealing temperature (T/T_m) for several nc metals. As is clear, the higher the homologous temperature is, the higher the instability of the grains and the larger the gain size is.

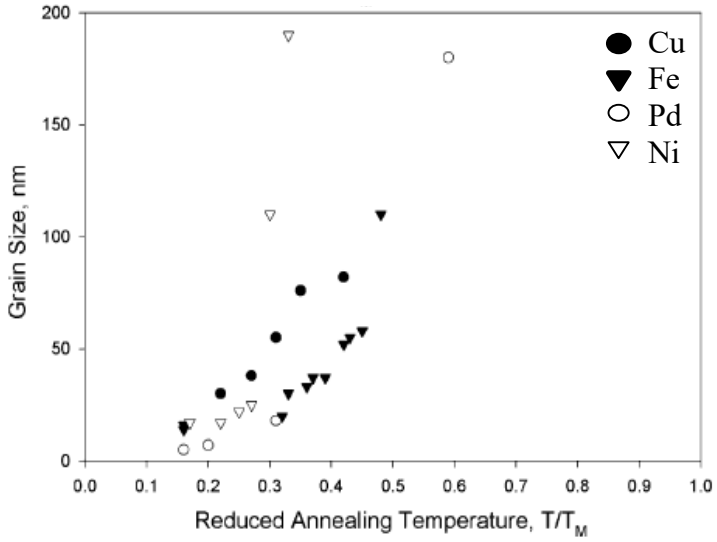

Figure 2. 8. Grain size versus reduced annealing temperature (T/TM) for Cu ⭘, Fe▼, Pd○, and Ni▽ [7]

The velocity of a grain boundary undergoing grain growth, equation 2.4 [79], is a function of both mobility and the curvature driven pressure:

$$v = M.P = M_O e\left[\frac{-Q}{RT}\right].\frac{2\gamma_b}{r} \qquad \text{eq. 2.4}$$

Where M is mobility, M_O is mobility's pre-exponential factor, and Q is the activation energy for grain boundary mobility. From equation 2.4 it becomes clear that grain growth can occur at low temperatures in nc metals as the very small value of r compensates for the reduced mobility.

Manipulating the parameters in equation 2.4 allows for two approaches of thermal stabilization in nanomaterials [80]. The first is a kinetic approach which considers the M parameter by addition of solute atoms that will induce a drag force to reduce the grain boundary mobility. The second is a thermodynamic approach achieved by manipulating P, or more specifically γ_b, where the added solute atoms segregates to the grain boundaries to reduce the system's free energy, and hence the driving force for grain growth [7].

As a result, and in spite of the driving force for grains to grow, significant stabilization against grain growth has been reported for several nc materials. However, a key factor in both strategies to inhibit grain growth is the involvement of solute atoms, as was stated above. Hence all systems reported to have achieved thermal stabilization are multicomponent systems whether its alloys or materials that contained impurities [7], as

evidenced by the improved thermal stability of a number of nc alloys compared to their pure counterparts [76].

The phenomenon of grain growth and thermal instability of nc materials does not only limit their service temperatures, but also their unique technological applications as a consequence. Hence, it becomes demanding to create thermally stable nc alloys to be utilized for their exceptional properties.

2.4.2 Kinetic Stabilization Mechanisms

Grain growth kinetics or grain boundary mobility can be slowed down by applying a retarding force to its movement by several methods. The most famous ones are second phase pinning or Zener pinning [67] and solute drag [81].

2.4.2.1 Solute Drag Effect

The influence of solute drag stabilization on grain boundary migration and hence grain growth is directly related to whether grain boundaries can escape or not be affected by the solute/impurity atmosphere. This can be explained by the two resultant opposing forces: the drag force exerted by the solute atoms and the driving force for grain growth. If solute/impurity drag force is considered, two situations can rise. For example, a low solute/impurity concentration would exert trivial opposition to the mobility of the boundary, leading to grain growth. However, grain boundary mobility drops if it faces a heavier obstacle as a result of increasing solute/impurity concentrations, hence impeding grain growth. On the other hand, considering the driving force for grain growth can yield

two other scenarios. A low driving force for grain growth suggests a lower grain growth rate, giving solutes/impurities sufficient time to diffuse to the grain boundary, reducing its mobility as it expands. In the case of smaller grains, such as in nanocrystallines, the driving force for growth is higher and continues to increase, as can be concluded from equation 2.3, leading to a much faster growth. As a result, solutes/impurities have less time to diffuse to the now longer paths. Still, at higher temperatures, diffusion of solutes/impurities is thermally enhanced and hence solute/impurity drag can take place. The exact scenario that can take place and the effect of the pinning pressure depends on solute-solvent interactions [82], [83].

A famous example of grain growth inhabitation by solute drag is reported by Michels et al. for Pd-19 at. %Zr alloy [81]. Even though the alloy was annealed up to 600^{o}C, nanocrystallinity was maintained and a grain growth from 5 nm to 16 nm was reported along with an increase in Zr concentration along the grain boundaries. This increase in Zr concentration, which is believed to have thermally stabilized the grain size, can be attained by either the diffusion of solute atoms from the lattice to the grain boundaries or through solute entrapment by the grain boundaries as they grew. However, as 600^{o}C represented only 47% of the melting temperature of the alloy, it was concluded that the temperature was too low for significant lattice diffusion to occur, and the increase in solute concentration in grain boundaries was attributed to solute drag.

In addition, a more recent study by VanLeeuwen et al. [84] used the predictions of a segregation model to prove that thermodynamic stabilization is not applicable for the

thermal stability of Pd-19 at.% Zr. Hence, authors concluded that the stabilization is due to Zr solutes up to about 700°C, while above this temperature significant growth is observed as seen in the TEM micrographs in Figure 2.9.

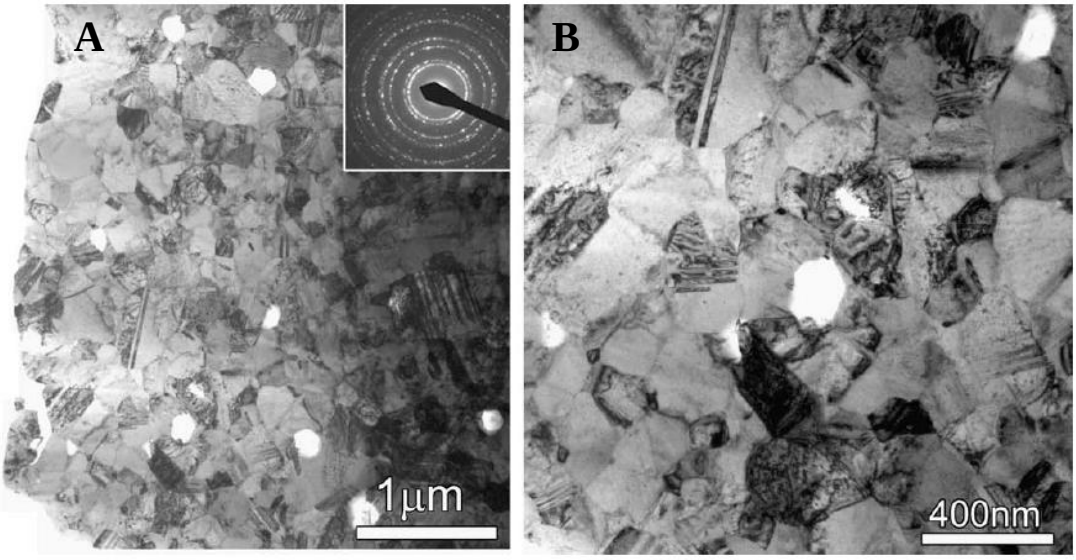

Figure 2. 9. Low magnification (a) and high magnification (b) of TEM micrographs of annealed Pd-19at%Zr at 950°C for 1 h [84]

In another example for solute drag stabilization, Knauth et al. [85] studied the effect of adding 1 at.% Si to Ni showed the difference in grain growth kinetics due to solute additions as a slower rate of growth was reported in the Ni-1 at.% Si at higher temperatures. The authors concluded after a series of calculations that solute diffusion could not be justified for the used time and temperature, and that the existence of Si in the

grain boundaries is rather due to its entrapment during grain boundary expansion, or in other words due to solute drag.

Zhou et al. [62] studied grain growth and thermal stability in a 26 nm nc Al synthesized by cryogenic mechanical milling. A grain size of 50 nm was obtained up to 74% of the metal's homologous temperature. Figure 2.10 shows the TEM micrographs of nc Al as milled and annealed at 673 K. The thermal stability was attributed to solute drag rather than Zener pinning as authors suggested the volume fraction of the second phase precipitates such as aluminum oxide and aluminum carbide was too low for significant pinning of the grain boundary migration.

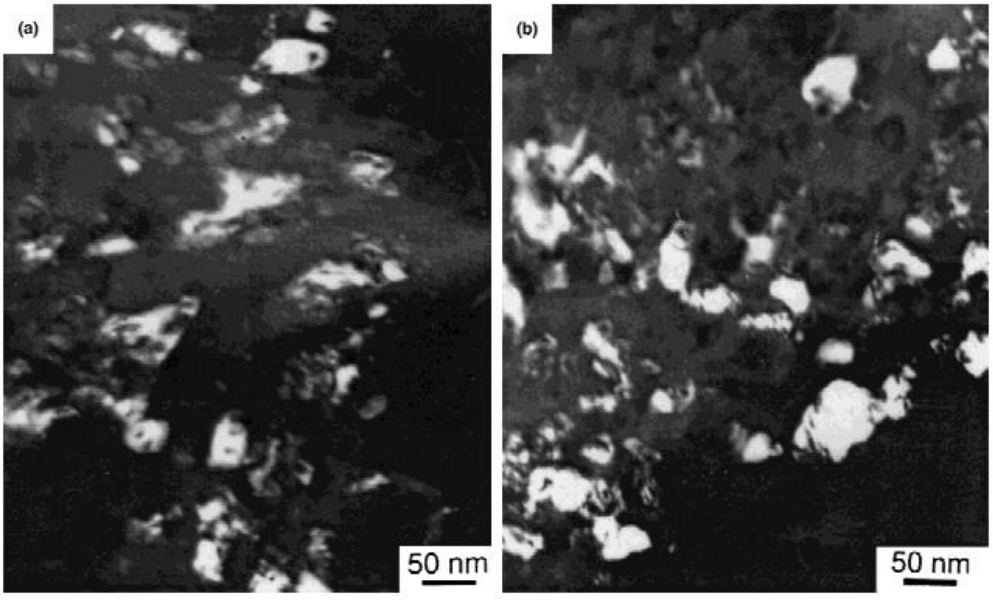

Figure 2. 10. TEM micrographs of as-milled nc Al (a) and annealed at 673 K for 200 minutes (b) [62]

2.4.2.2 Second Phase Pinning (Zener) Effect

In case of the solute atoms forming second phases, whether it is in the form of precipitates or dispersoids, impeding grain boundary movement is said to be due to the pinning pressure of the Zener drag mechanism described by [86]:

$$P_Z = \frac{3F\gamma}{2r} \qquad \text{eq.2.5}$$

Where P_z, F, r, and γ, are the pinning pressure applied by the second phase particles, their volume fraction, their radius, the specific grain boundary energy, respectively. For P_z to successfully pin down the grain boundary movement, it must overcome the grain boundary pressure given in equation 2.3. To do so, as can be concluded from equations 2.3 and 2.5, either a very small radius is required for the second phase particles or a very high volume fraction, in order for P_z to be greater than P. Zener pinning effect is less temperature sensitive than the solute drag effect as it is capable of yielding thermal stability at very high temperatures, yet this effect must be controlled by the solid solubility limit of the second phase particles and their diffusivity at high temperatures. This is because dissolution or grain coarsening of these particles at high temperatures will eliminate its role in grain boundary stabilization.

This mechanism has been reported to be successful in the stabilization of several nc systems. Shaw et al. [11] studied the thermal stability of $Al_{93}Fe_3Ti_2Cr_2$ alloy synthesized by mechanical alloying. Thermal stability up to 77% of the alloys homologous temperature was reported. The authors accredited the initial stability of the alloy to solute

drag mechanism, however at higher temperatures than 450°C, the formation of several second phases or intermetallic compounds starting with Al_6Fe and followed by Al_3Ti, $Al_{13}Fe_4$, and $Al_{13}Cr_2$, assured the contribution of Zener drag mechanism.

A recent study of cryomilled nc Cu reported by Atwater et al. [64] has also shown an enhanced thermal stability up to 900°C due to the addition of only 1 at.% Zr. The stability was justified by the Zener pinning mechanism due to the presence of ZrO_2 and Cu_5Zr at higher temperatures. This was supported by the TEM bright field micrograph and diffraction pattern of Cu-1 at.% Zr annealed at 900°C shown in Figure 2.11, where innermost diffraction rings are seen in addition to the Cu rings. In addition, measurements from the bright field TEM micrograph reported a volume average grain size of 59 nm.

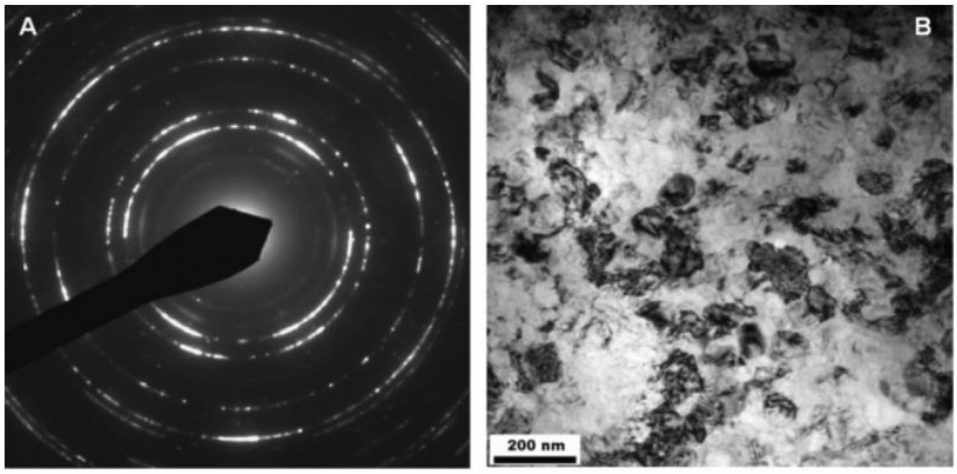

Figure 2. 11. TEM diffraction pattern (A) and bright field micrograph (B) of Cu-1at%Zr annealed at 900°C [64].

In another example for Cu stabilization, Youssef et al. [65] reported that the addition of 1%Nb to nc Cu kinetically stabilized the nanostructure against grain growth. Authors suggested that the dominant mechanism for stabilizing the Cu nanostructure at lower temperatures is solute drag. However, the precipitation of nano Nb atoms at high annealing temperatures near the Cu grain boundaries, as evident by the Nb (110) ring seen in the diffraction pattern in Figure 2.12, indicates the contribution of Zener pinning where the nanoprecipitates acted as a frictional force to oppose boundary motion.

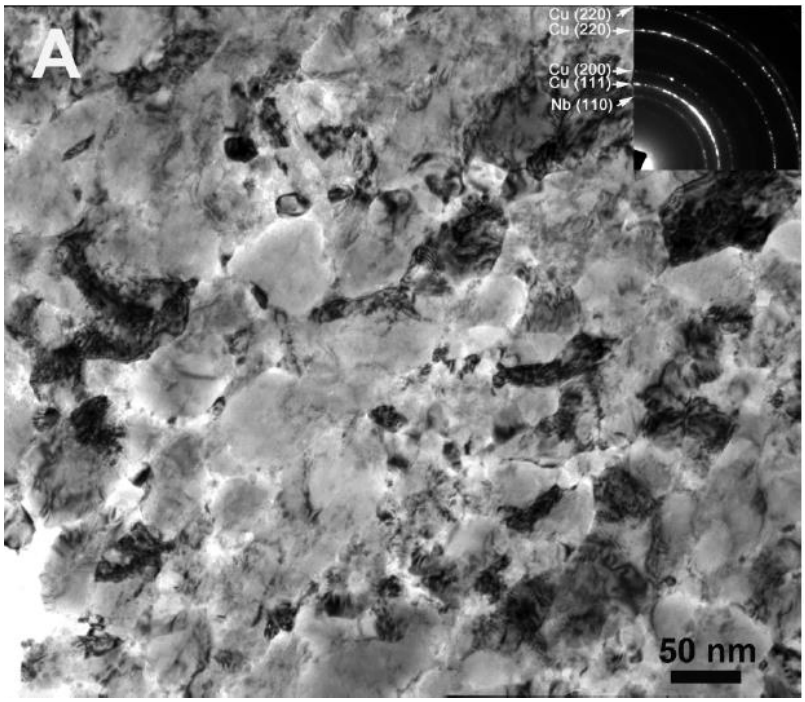

Figure 2. 12. Bright-field TEM micrograph for nc Cu-1% Nb and the diffraction pattern (upper right) after annealing at 1073K for 1h [65]

Other examples of thermal stabilization by Zener pinning in nc systems include nc Al due to precipitation of Al_2O_3 and Al_4C_3 [10], Al–7.5 wt.% Mg due to precipitation of Al_2O_3 and Al_4C_3 [63], Ni-1.2 at.% P due to precipitation of Ni_3P [67], Fe-10 wt.% Al due to precipitation of Al_2O_3 [69], Mg–12 wt.% Cu due to precipitation of Mg_2Cu [71], and Cu-10 at.% W due to precipitation of W [66].

2.4.3 Thermodynamic Stabilization Mechanisms

Eliminating the driving force for grain growth as a result of decreasing the overall free energy of the system can be achieved by reducing the grain boundary energy, instead of dealing with reducing the grain boundary mobility. This approach is the route for the thermal stability in the thermodynamic mechanism. Still, addition of solute atoms is significant to this mechanism, as was stated earlier, where such atoms must have a high tendency to segregate to the grain boundaries to reduce the driving force for grain growth [7]. The relationship between the segregated solute atoms and the grain boundary energy is expressed by solving the Gibbs adsorption equation, given by equation 2.6, in the dilute limit [87] to yield the grain boundary energy after solute segregation, γb, as a function of the segregated solute content at temperature, T, given by equation 2.7 [87].

$$d\gamma = -\Gamma_A d\mu_A \qquad \text{eq. 2.6}$$

Where γ is the grain boundary energy, μ_A is the chemical potential of solute atoms, and Γ_A is the amount of solute atoms segregated to the grain boundary.

$$\gamma = \gamma_O + \Gamma_S [\Delta H_{seg} - T\Delta S_{seg}] \qquad \text{eq. 2.7}$$

Where γ is the grain boundary after segregation, γ_O is the grain boundary energy before segregation, Γ_s is the segregated solutes, T is absolute temperature, and ΔH_{seg} and ΔS_{seg} are the change in enthalpy and entropy due to the segregation of solute atoms from lattice sites to grain boundary sites, respectively.

According to equation 2.6, increasing the solute content leads to reducing the grain boundary energy. This trend is reported to strongly hold in the presence of a large atomic misfit between the solute and host atoms, suggesting that the segregation to grain boundaries is induced by the elastic strain energy. This is because the excess free volume in the grain boundaries permits the largely misfit solutes to release the elastic strain associated with the large size misfit due to being in the lattice. At the same time, if the solute atoms have a high tendency towards grain boundary segregation, the amount of solute that segregates upon annealing or at higher temperatures increase, which leads to decreasing the grain boundary energy eliminating the need for grain growth [88]. From equation 2.7, it is clear that for solute segregation to be favored to produce γ less than γ_O, $[\Delta H_{seg} - T\Delta S_{seg}]$ must be less than zero. These concepts have been developed and modeled by Weissmuller [87], Liu and Kirchheim [89], Millett et al. [75], Trelowitz and Schuh [76], Chookajorn et al. [90], and Saber et al. [91].

Thermodynamic stabilization was reported in several nc alloy systems such as Ni–P [92], RuAl with Fe solutes [93], Y–Fe [94], and TiO_2 with Ca additions [95]. In all of these systems, authors attributed the grain size stability to the lowering of the grain boundary energy as a result of solute segregation to the grain boundaries. In cases where

precipitation of second phases and solutes may have occurred at higher annealing temperatures, grain growth is observed and stability is lost. This indicates that the loss of solutes from the grain boundaries of these systems had a more profound effect on the loss of thermal stability, than the stability that could be obtained by the second phases [7].

2.4.4 The Proper Dopant for Thermodynamic Stabilization

The ability to produce bulk materials that maintain its nanostructure and hence its enhanced mechanical properties is dependent on the thermal stability of the material. Hence the first goal before successfully utilizing nano materials in a variety of promising applications, trace addition of a suitable alloying element (dopant) that will segregate to grain boundaries and stabilize the grain size in Al and Al-Li alloys to high temperatures is to be chosen.

The selection of a dopant suitable for thermodynamic stabilization requires consideration of elastic and chemical contributions in equation 2.7. Solute segregation to free surfaces can be represented by the Wynblatt-Ku (WK) model [96]. The model is based on a nearest-neighbor regular solution model and the required parameters can be found in literature. Replacing the single monolayer interface with a double monolayer interface allowed for deriving a modified version of this model, where the interface bonds account for the grain boundary energy. The change in the enthalpy of segregation is given as a linear combination between: The chemical enthalpy $\Delta H_{chem,}$ and the elastic enthalpy of segregation, ΔH_{els} [96].

$$\Delta H_{seg} = \Delta H_{chem} + \Delta H_{els} \quad \text{eq. 2.8}$$

Where:

$$\Delta H_{chem} = (\gamma^s{}_A - \gamma^s{}_B)(1-\alpha)\sigma - \frac{8\Delta H_{mix}}{Z}[Z_{in}(X^*{}_A - X_A) - Z_{out}(X_A - 0.5) + \alpha Z_{out}(X^*{}_A - 0.5)] \quad \text{eq. 2.9}$$

A or B denote solute or solvent atoms, γ^s is the surface energy, σ is the molar interfacial area, Z, Z_{in} and Z_{out} are coordination numbers for bulk, in-plane and out-of-plane interface bonds, X_A and X^*_A are the equilibrium bulk and interfacial solute atom fractions, ΔH_{mix} is the equimolar ($X_A = X_B$) enthalpy of mixing in the liquid state, and α is the ratio of interface/bulk bond strengths. If α = 0, the WK result in reference [39] for free surface segregation is obtained. It is assumed that $\gamma_b = \gamma^s / 3$, which requires α = 5/6 with $Z_{in} = Z/2$ for evaluation purposes. $\sigma = V_B^{2/3} N_{AVG}$, where V_B is the atomic volume and N_{AVG} is Avogadro's number.

ΔH_{el} is the enthalpy contribution from the solute misfit elastic strain energy $\Delta E_{el} \geq 0$. For oversize solutes, grain boundary free volume will accommodate the misfit and segregation is favored, i.e., $\Delta H_{el} = -\Delta E_{el}$ in equation 2.8. Equation 2.8 provides a basis for comparing the effect of candidate solutes for thermodynamic stabilization in Al-base alloys. In addition it gives useful insight on the interplay of the various parameters involved. Only oversize solutes with very low equilibrium solubility in Al are considered

($X_A = 0$) since we do not want dopants that can be major alloying components. Equation 2.8 can be combined with equation 2.7 using $\Gamma_s = 2\,X^*_A/\sigma$ (double monolayer) to give:

$$\gamma_{Al} = \gamma_o + \frac{2X^*_A}{\sigma}\left[\frac{\gamma^S_A - \gamma^S_{Al}}{6}\sigma - \frac{\Delta H_{mix}}{3}(17X^*_A + 0.5) - \Delta E_{el}\right] \qquad \text{eq.2.10}$$

The entropy of segregation (ΔS_{seg}) makes only a small contribution when ΔH_{seg} is large and is ignored in equation 2.10.

Based on the thermodynamic models discussed above, different solutes were tried in Al and we found out that Strontium (Sr) in Al demonstrated significant stability, thereby holding the promise for facilitating production of bulk parts with nanostructures. Figure 2.13 is a plot using equation 2.10 for the solute-segregated grain boundary energy (γ_{Al}) vs. the atom fraction of Sr solute X^*_{Sr} on the boundary. The trend in such model is the significant point. Li should have a negligible influence on thermodynamic stabilization relative to a dopant (Sr). A negative enthalpy of mixing will result in a minimum in the curves and the relative magnitudes of ΔH_{el} and ΔH_{mix} determine whether or not the $\gamma_{Al} = 0$ intersection occurs, i.e., complete thermodynamic stabilization is achieved, as shown in Figure 2.13.

In addition, the thermodynamic model can also predict the minimum grain size of stabilization, which follows directly from a solute mass balance. Figure 2.14 shows the minimum grain size for stabilization in Al-Sr system with different concentrations of Sr as a function of annealing temperature. In this thesis, 1 at.% Sr is added to study its effect experimentally on stabilizing nc Al and nc Al-Li alloys.

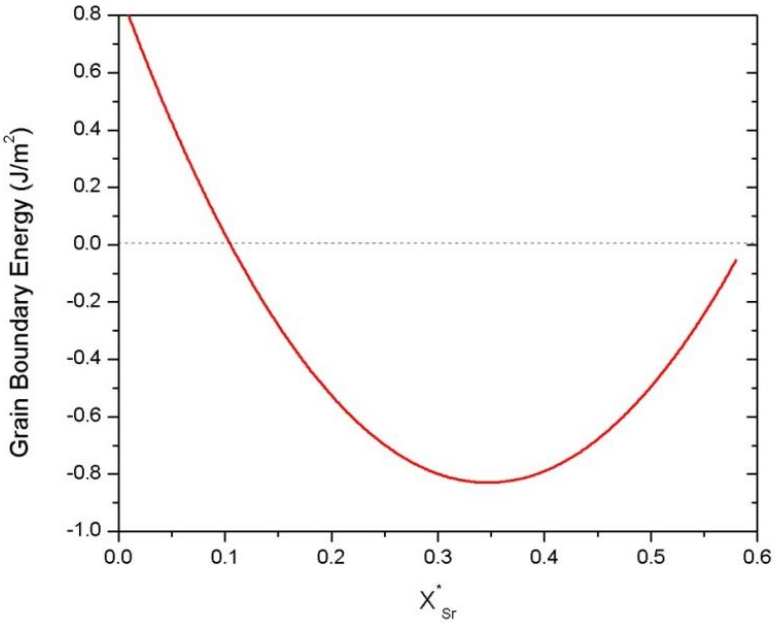

Figure 2. 13. Grain boundary energy vs. the atom fraction of Sr.

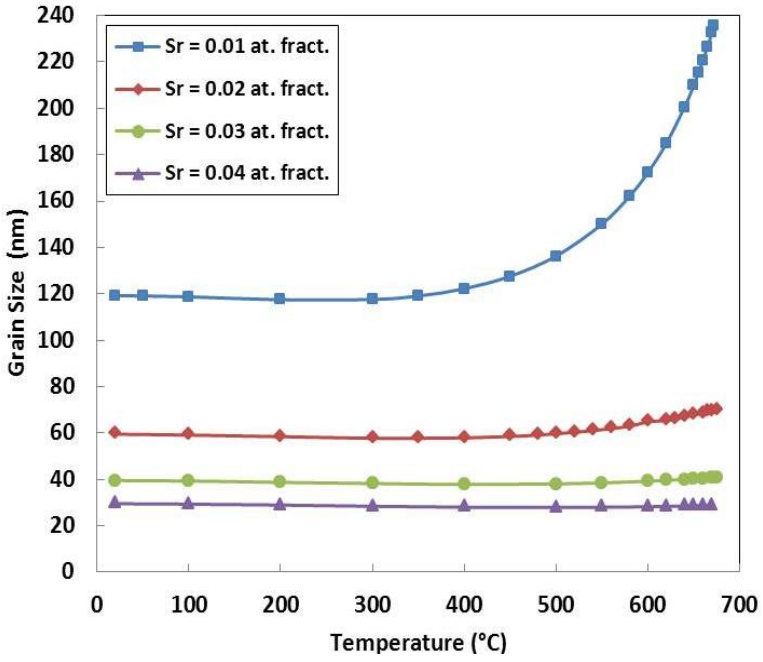

Figure 2. 14. Thermodynamic stabilization of Al grain size as a function of temperature at different Sr content.

Chapter 3. Experimental Procedures

The experimental procedures conducted for this thesis are presented in this chapter and are divided into two main sections. The first section describes the preparation of the nc samples including pure nc Al, nc Al-1 at.% Sr and nc Al-2 at.% Li-1 at.% Sr. It starts with the mechanical milling of the powders, to annealing it at several temperatures for testing its thermal stability, and finally compacting it into disks for experimental characterization. The second section is the experimental characterization section which includes the structural analysis conducted such as x-ray diffraction (XRD) and transmission electron microscopy (TEM). As well as the mechanical properties analysis which includes Vickers hardness, shear punch, and scanning electron microscopy (SEM).

3.1 Sample Preparation

3.1.1 Mechanical Milling/Alloying of Powders

Elemental powders of Al, Li, and Sr were used with purity of 99.97%, 99.99%, and 99.95%, respectively, were used and sealed in a steal vial along with the stainless steel balls under ultrahigh purity argon atmosphere (UHP) (O_2 < 1ppm). The synthesis process is carried in a SPEX 8000 shaker-mill model and cryomilled or mechanically milled at liquid nitrogen temperature. This was done by using a specially designed nylon vial holder with liquid nitrogen flowing around it to maintain its temperature at about 77 K. This is to avoid welding of ductile Al during the synthesis process.

The ball-to-powder mass ratio used is 20:1 and the powders were cryomilled for 6 hours. A detailed mechanism for producing nano-sized grains via mechanical milling is described in section 2.3. As the vial's temperature was kept at liquid nitrogen temperature for the entire milling duration, no thermal recovery of the grains is possible and the attained nc grain size is the result of the high density of dislocations created which eventually combines to form the nano-sized grains. At the end, three as-milled samples were prepared which includes nc Al, nc Al-1 at.% Sr, and nc Al-2 at.% Li-1 at.% Sr. To test for the purity of the as-milled powders, the samples were analyzed by Luvak Inc.

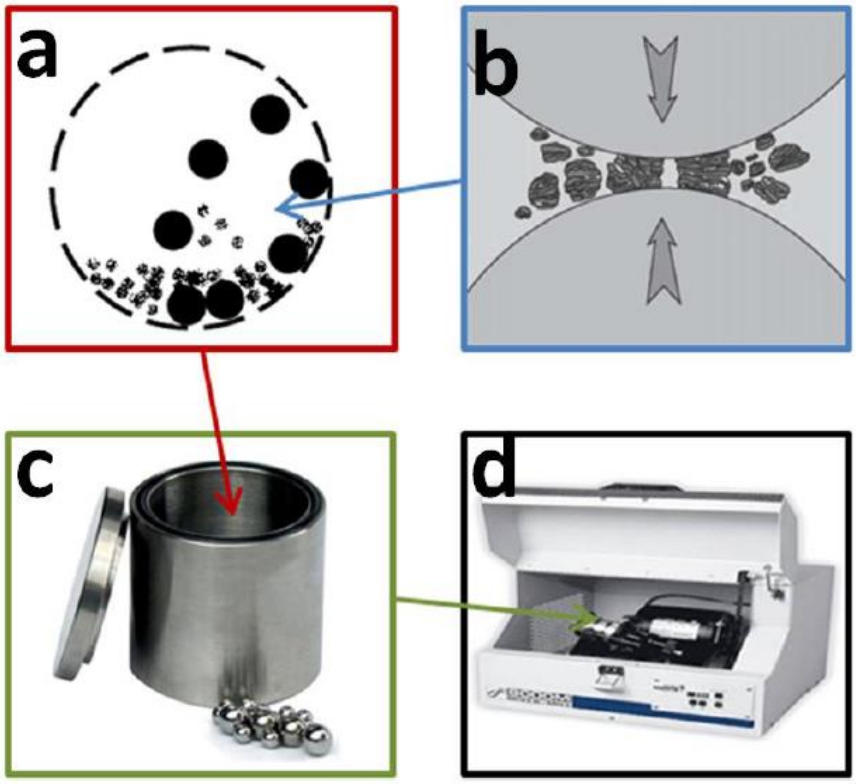

Figure 3. 1. Representation of the milling process

3.1.2 Annealing Heat Treatment

The as-milled powders were isothermally annealed starting from 573 K up to 773 K for 1 hour, and at 873 K, which represents 94% of the samples homologous temperature, for 1 hour and 24 hours to test the thermal stability of the prepared samples.

Lindberg tube furnace with a 2” diameter is the furnace used for annealing the samples for this study. The powders were placed into a quartz tube along with a thermocouple and vacuum was applied to push the air out of the tube furnace. After that the tube was refilled with 98% Ar + 2% H_2 gas and the process of evacuating and refilling was repeated at least three times to insure an O_2 free atmosphere.

Before inserting the tube inside the furnace, the furnace controller would be set to the required temperature and allowed to stabilize. After annealing for the desired time, the tube was moved out of the furnace and is air cooled to room temperatures before taking out the samples.

3.1.3 Consolidation of Powders

In order to test for the mechanical properties, the as milled and annealed powders must be compacted into bulk samples that obtain a theoretical density. To do so, our powders were green compacted, that is without the use of heat, in order to form disk-shaped specimens. This was done via uniaxial cold pressing at 1 GPa in a 6.35 mm tungsten carbide die such as the one shown in Figure 3.2 B & C, along with a picture of the compacting equipment used (Figure 3.2 A). After compaction, all samples were hand polished to obtain smoother surfaces.

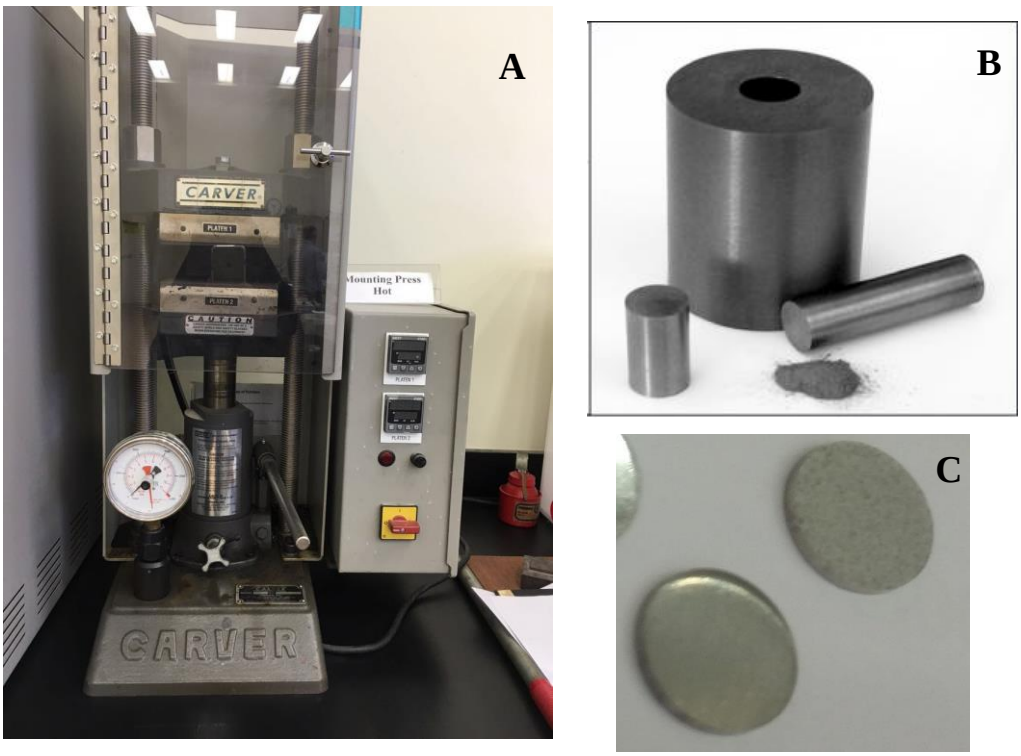

Figure 3. 2. Compacting equipment (A), compacting die (B), and compacted disks (C)

3.2 Characterization Methods

3.2.1 Structural Analysis

The structural analysis involves the studying of the microstructure of the nc powders of both as milled and annealed samples. This is mainly done for two reasons: the first is to calculate or measure the average grain size for the different specimens, and the second is to identify the structures and hence the phases present in the samples. This analysis is done in order to study the thermal stability by comparing the effect of the added Sr and whether it has helped in maintaining the grain size in the nano range.

3.2.1.1 X-Ray Diffraction (XRD)

X-ray diffraction method is known to be one of the most basic yet a very important non-destructive structural analysis technique used in the characterization of crystals. This is due to its ability to be used in the determination of several important features such as the crystal structure, the phases present, the lattice constant, and the grain size and lattice strain [97]. The main principle behind how this technique functions is basically presented in Bragg's law given by equation 3.1 and schematically illustrated in Figure 3.3. It can be explained as the following: An x-ray beam with wavelength λ that hits the planes of a crystalline material with a certain angle, the rays will only diffract if the difference in the distance traveled by the rays that are reflected from successive planes equals a complete number n of wavelengths, that is when it satisfies by the Bragg condition [97].

$$n\lambda = 2dsin\Theta \qquad \text{eq.3.1}$$

Where λ is the wavelength of the x-ray beam, d is the inter-planar spacing and Θ is the angle. This allows the identification of different structures and different phases according to their diffracted planes.

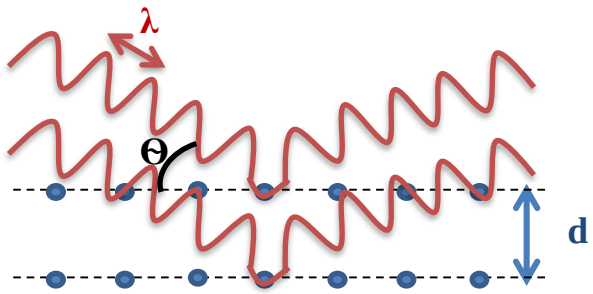

Figure 3. 3. Schematic representation of Bragg's law

For this thesis, a Rigaku X-ray diffractometer, shown in Figure 3.4, was used in the analysis of our disk compacted as-milled as well as annealed samples with CuKα (λ = 0.1542) radiation. The instrument was used at 30 kV and 15 mA and programmed to proceed with the following parameters: A step size of 0.01^{O}, dwell time of 1 sec, and a scan range of $20\text{-}100^{O}$.

In a diffraction pattern, the broadening of the peaks is the result of several factors which are the grain size, the stored strain within the grains, and other instrumental factors. An accurate estimation of the grain size requires the subtraction of the instrumental contribution to the broadening of the peaks from the total broadening [97]. This was done

by the software by using an annealed standard alumina sample and assuming a Gaussian peak shape.

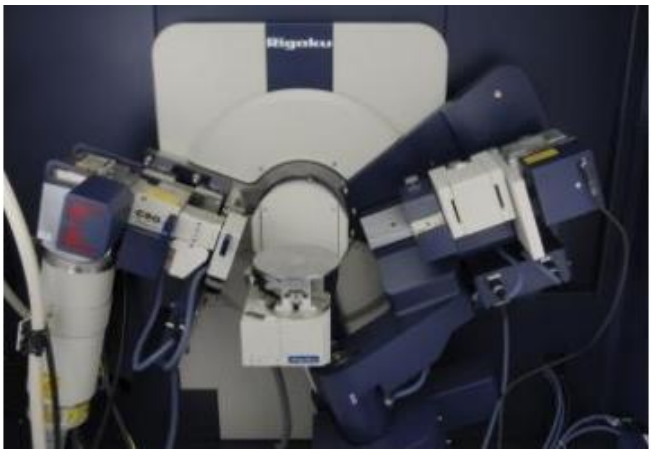

Figure 3. 4. Rigaku X-ray diffractometer

The positions of the peaks from the diffracted atomic planes allows for the identification of the phases present. In addition, the broadening of the peaks of the XRD patterns can indicate the range of the grain size even before calculations are conducted. This is because the grain size refinement and the introduction of lattice strain during the milling process can be interpreted by the XRD pattern, where the smaller the grains are, the larger the broadening of the peaks and the lower their intensities are [98]. The XRD line broadening was used to calculate the average grain size and lattice strain using the integral breadth analysis and the Averbatch formula given by equation 3.2 [98].

$$\frac{\beta^2}{tan^2\theta_o} = \frac{\lambda}{d}\left(\frac{\beta}{\tan\theta_o \sin\theta_o}\right) + 25\ e^2 \qquad \text{eq.3.2}$$

Where β is the measured integral breadth, or in other words it is the full width half maximum (FWHM) of the peak, θ_o is the peak's diffraction angle, λ is the x-ray wavelength of 0.154 nm, d is the average grain size, and e is the lattice strain. FWHM and θo were found for each peak by individually plotting each peak in OriginPro analysis software and fitting them with a Gaussian fit. Another use for the XRD patterns was to calculate the lattice parameter which was done using the Cohen method [99] given by equation 3.3.

$$a = a_o + a_o k cos^2\Theta \qquad \text{eq.3.3}$$

Where a is the lattice parameter calculated at each peak, a_o is the average lattice parameter and Θ is the peak's angle.

It is always recommended to perform transmission electron microscopy in conjunction with XRD when analyzing nanomaterials for grain size for more valuable and reliable results.

3.2.1.2 Transmission Electron Microscopy (TEM)

Transmission Electron Microscopy (TEM) is a crucial technique for the characterization of nanomaterials. It serves as a method that provides quantitative measures of grain size and its distribution, due to its capability of directly imaging nanoscale grains. This is done by focusing a beam of electrons through thin samples and imaging the transmitted beam to form an image, enabling it to obtain a resolution much higher than that obtained by a light microscope. This advantage is related to the main concept behind the TEM's working principle, that is using a beam of electrons which have small wavelengths which allows viewing objects much smaller than those that can be resolved using visible light [100].

Due to this fact, TEM is a crucial and sometimes mandatory characterization technique that has become an integral part of materials science in the fields of nanotechnology and low dimensional materials.

One factor upon which successful imaging of nanoparticles using TEM depends on is the contrast of the sample relative to the background. The sample thickness (the amount of material the electron beam passes through) as well as the sample material (the electron mean free path in heavier atoms is smaller than that in lighter atoms as less scattering can occur by the later atoms) are two factors upon which the contrast is based. Hence there are two modes in which imaging can take place in a TEM, dark field mode (where the background is dark and particles or grains are light in color) or bright field mode (where the background is light and particles or grains are dark in color) [100]. Detailed

explanations of the equipment setup, the theory of the technique, and terminology can be found in any TEM text book including [100].

Using TEM to match grain size results and other structural information obtained by a simpler method such as XRD has proven to be very valuable. This holds as the TEM method can perform as a measuring tool rather than a mathematical calculation method to support the XRD grain size calculations. XRD method was used in the grain size calculations for each sample, however a more demanding TEM technique was used to verify chosen samples to validate the XRD results.

Before characterizing materials with TEM, a non-trivial sample preparation process must take place. Chosen samples, whether as milled or annealed, had to be compacted into thin disks of 3mm diameter by uniaxial cold pressing at 3 GPa in a tungsten carbide 3 mm diameter die, then polished by hand to ~100µm thickness. After that, the disks were placed into the sample holder of a Fischione double-jet electropolisher, shown in Figure 3.5, and electropolished with 10 vol% perchloric acid in ethanol at 0 °C.

The main concept behind the double-jet electropolisher is to pump a flow of negatively charged electrolyte onto the surface of a positively charged sample until a small hole is created in the center of the sample. Above one jet nozzle, a light bulb is attached while above the other jet nozzle, a photodetector is attached. The two are attached to optic fibers that are opposite to each other and continue along the jet stream from both sides of the sample. Once the hole is created, the optic fibers allow the light to be transferred from the light bulb to the photocell and an alarm is released. Once this occurs, the process

should be terminated immediately in order to prevent further damage to the sample [101].

Figure 3. 5. Fischione double-jet electropolisher

The prepared samples were finally analyzed using a JEOL 2000FX TEM system, shown in Figure 3.6, operating at 200kV and linked to the Digital Micrograph software to calibrate the micrographs. Bright field and dark field TEM micrographs were obtained in order to study the microstructure of the nano-grained samples to determine the average grain size as well as the grain size distribution. The data analysis was done using ImageJ software using the line function and measuring two directions perpendicular to each other before taking the average. This was done to 200 grains to insure more reliable results.

In addition to the data obtainable by the micrographs, selected area diffraction (SAD) patterns can be obtained which give structural information and allow for secondary phase identification in a concept similar to that in the XRD. However instead of peaks, spots that correspond to a satisfied diffraction condition of the sample's crystal structure appear. In the case of nc materials, rings rather than spots appear due to the smaller grains size which allows for a larger number of grains to be detected each with its own plane orientation, which in turns form a ring at the same distance from the center [100].

Figure 3. 6. JEOL 2000FX TEM system

3.2.2 Mechanical Properties Analysis

In order to verify whether the added Sr had indeed stabilized the nc Al and the nc Al-Li alloy, not only the size but more importantly the exceptional mechanical properties that are obtained in the nano-regime must still persist along the range of temperatures tested. Hence this section sheds the light on the mechanical analysis conducted to test for both hardness and ductility of our as milled and annealed samples.

3.2.2.1 Vickers Hardness

Vickers micro-hardness test is an inexpensive and a reliable method for evaluating basic mechanical properties. It is considered one of the most important, non-destructive, and widely-used characterization procedure in both the metal industry and in research [102]. Not only does it test for the hardness of materials, but gives a general understanding or estimation of the tested material's strength due to the general relation between a material's hardness and its yield stress given by Tabor's relation [103].

Hardness tests are done by measuring the size of the plastic impression left as a result of an indenter load in the sample. While load is being applied to the indenter, the depth of penetration or impression beneath the surface is measured as the geometry of the indenter is known, making it possible to determine the size of the area of contact. The softer the material is, the deeper the indentation and the lower its yield strength is [102].

The Vickers indenter has a pyramid shape with a square base. After a certain load is applied on the sample tested for a specific amount of time, the load is released and a

diamond shaped indent with diagonals d1 and d2 is left behind. The diagonals are then measured with the aid of a microscope attached to the instrument along with the hardness [102].

Our hardness measurements were carried out using a Future-Tech Microhardness Tester FM-800 shown in Figure 3.7. The automated loading system was used with 5-10 seconds dwell time. A 25 g load was applied on the 6.35 mm diameter and 1 mm thick disks with a total of five indentations on each sample to obtain an average and calculate the standard deviation.

Figure 3. 7. Future-Tech Microhardness Tester FM-800

3.2.2.2 Shear Punch

The shear punch test or SPT is a mechanical properties characterization method used when evaluating small test samples. In this test, a flat cylindrical punch is driven through the sample to be tested which is clamped between two dies. As a result, the punched area is deformed and a circular disk is punched out from the sample [104]. During punching, the load applied on the punch is recorded as a function of the punch displacement resulting in a shear stress vs. displacement curve. Figure 3.8 shows the setup used along with a schematic of the shear–punch test geometry [105].

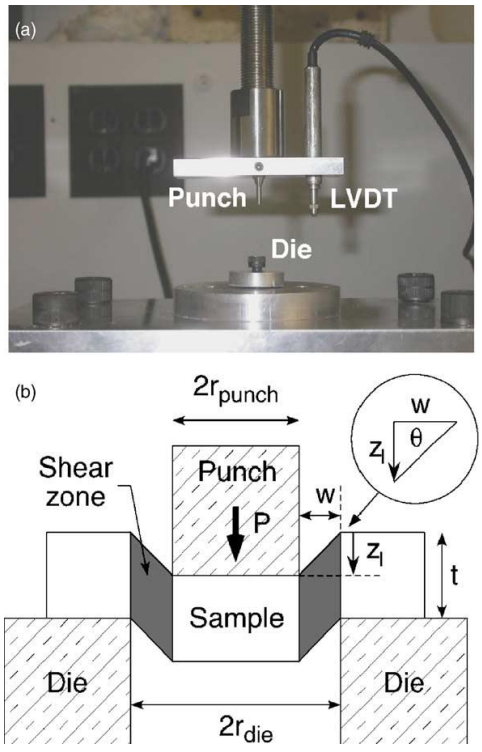

Figure 3. 8. Set up of the shear punch test

In this work, SPT was used in order to create deformation in our samples to check for the ductility of our nc Al and Al alloy samples after stabilizing its grains sizes. Samples to be tested where compacted into 5mm diameter in tungsten carbide dies under an applied uniaxial pressure of 3GPa, then hand polished to 250-300 μm thickness. SPT was run at a speed of 0.01 mm/min and a punch diameter of 100 μm. After SPT, SEM was conducted on selected samples to verify the SPT calculations by studying the ductility through examining the shear punched samples' fracture surfaces.

3.2.2.3 Scanning Electron Microscopy (SEM)

Another electron microscopic technique that was used in the characterization of our samples is the scanning electron microscope (SEM). Just like the TEM, the SEM has the advantage of high resolution and magnification due to the small wavelength of electrons. However in this technique, an electron beam scans over the surface of specimens to create an image. This leads to an interaction between the electron beam and the atoms at various depths within the sample and produces several signals that are collected to generate an image of the surface and hence gain information about the surface topography and composition [106].

Different types of signals and detection modes can be generated by an SEM. The most common mode is called secondary electron imaging or SEI, where the interaction of the focused electron beam and surface of the sample, leads to the release of secondary electrons that are emitted from distances very close to the sample's surface. Hence, high resolution images of sample surfaces are obtainable by SEM, revealing details that are less than 1 nm in size. The details of the equipment and theory can be found in any SEM book such as [106].

For this thesis, FEI Nova NanoSEM 450 shown in Figure 3.9, was used to study the fracture surface of the samples that underwent the shear punch test to examine the samples ductility.

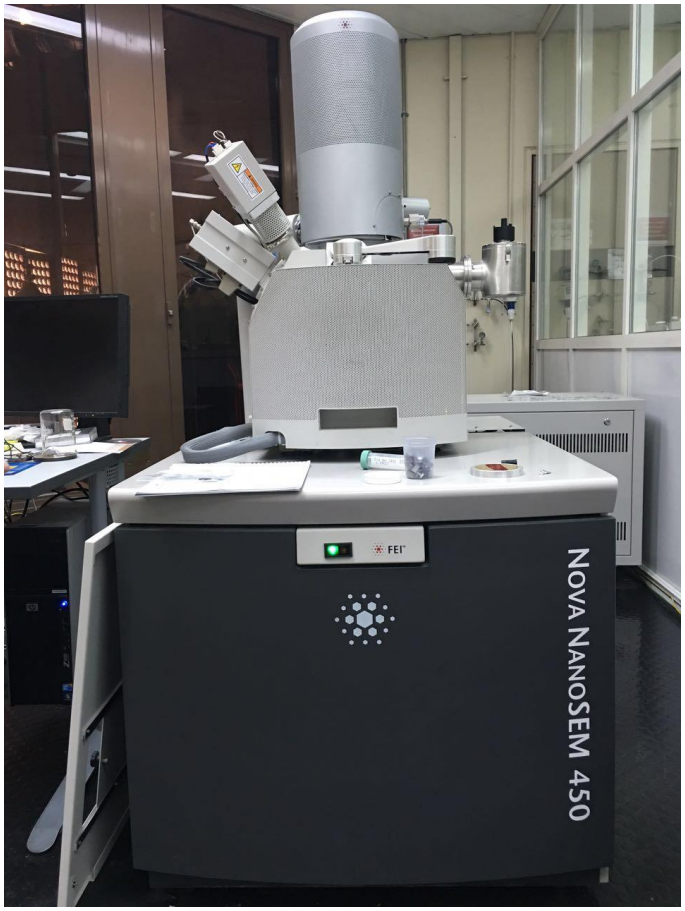

Figure 3. 9. FEI Nova NanoSEM 450

Chapter 4. Results & Discussion

4.1 Synthesis of Nanocrystalline Al

The success of synthesizing nc Al by mechanical cryomilling is the highlight of this section through studying its microstructure. In order to study the effect of adding Sr to nc Al, the behavior of nc Al needed to be studied first.

After cryomilling nc Al for 6 hours, its chemical composition was measured at Luvak Laboratory using an inductive coupled plasma (ICP)/Leco furnace and the results are shown in Table 4.1. As can be seen, no contamination from nitrogen is found due to the fact that liquid nitrogen was introduced outside the milling vial in our cryomilling process. In addition, contamination from the steel vial and the atmosphere is trivial as concluded by the reported 0.06% Fe and 0.13%O, respectively.

Table 4. 1. Chemical composition of the cryomilled nc Al (wt.%)

Element	O	N	Fe	Al
Wt.%	0.13	-	0.06	Balance

Figure 4.1 shows the XRD pattern of Al cryomilled for 6 hours. The positions of the peaks from the diffracted atomic planes indicate the presence of face-centered cubic (FCC) Al phase, as indexed on the pattern. For comparison, the XRD pattern of the coarse grained Al is shown in the same figure as well. Comparing the broadening of the peaks of nc Al and coarse grained Al, one can tell that the grain size of the as milled nc sample is smaller than that of the coarse grained Al. This is because the grain size refinement and the introduction of lattice strain during the milling process can be interpreted by the XRD pattern, where the smaller the grains are, the larger the broadening of the peaks, indicating a larger grain size for conventional grained Al [98].

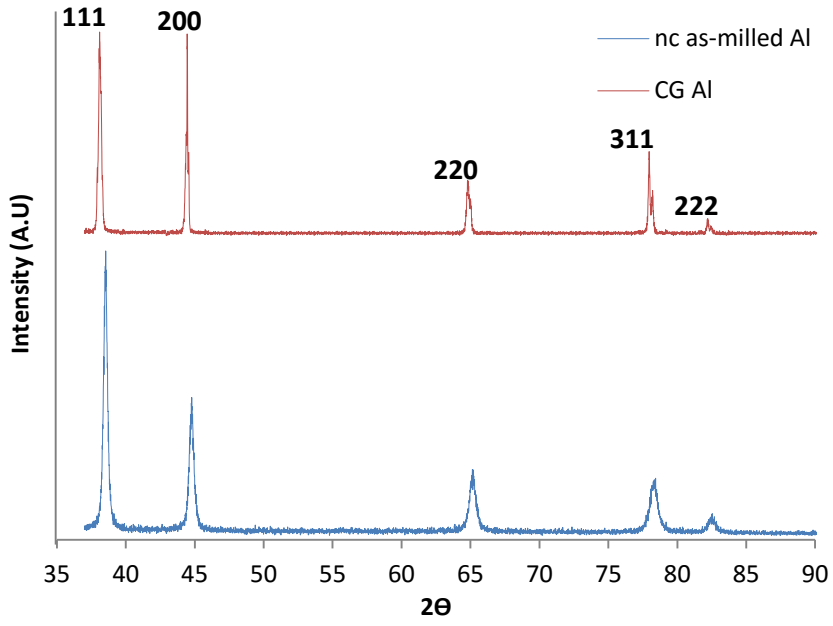

Figure 4. 1. XRD pattern for as-milled nc Al and coarse-grained Al

The XRD line broadening was used to calculate the average grain size and lattice strain of nc Al using the integral breadth analysis and the Averbatch formula [98] shown below.

$$\frac{(\beta)^2}{tan^2\theta_o} = \frac{\lambda}{d}\left(\frac{\beta}{\tan\theta_o \sin\theta_o}\right) + 25\, e^2 \qquad \text{eq.4.1}$$

Where β is the measured integral breadth, or in other words it is the full width half maximum (FWHM) of the peak, θ_o is the peak's diffraction angle, λ is the x-ray wavelength for Cu Kα of 0.154 nm, d is the average grain size, and e is the lattice strain.

Figure 4.2 shows the least squares fit of the $\frac{(\beta)^2}{tan^2\theta_o}$ vs. $\left(\frac{\beta}{\tan\theta_o \sin\theta_o}\right)$ obtained for all measured peaks. A 0.95 standard linear regression is obtained indicating a good fit. The average grain size and the lattice strain obtained by the Averbatch method of nc Al are 39 nm and 0.2%, respectively.

To verify grain size calculations and further study the microstructure, TEM was performed on the as-milled nc Al sample. Bright field and dark field TEM micrographs for the as milled pure nc Al are shown in Figure 4.3 A and B. The grains appear to be equiaxed with a random distribution within the structure, and with no evidence for abnormal nc grains. Figure 4.3 C shows the grain size distribution of nc Al based on measuring 200 grains form the DFTEM images. This figure indicates a monotonic distribution of grain size with a mean grain size value of 33±6 nm for as milled nc Al. This value is in a good agreement with the 39 nm grain size obtained by XRD calculations.

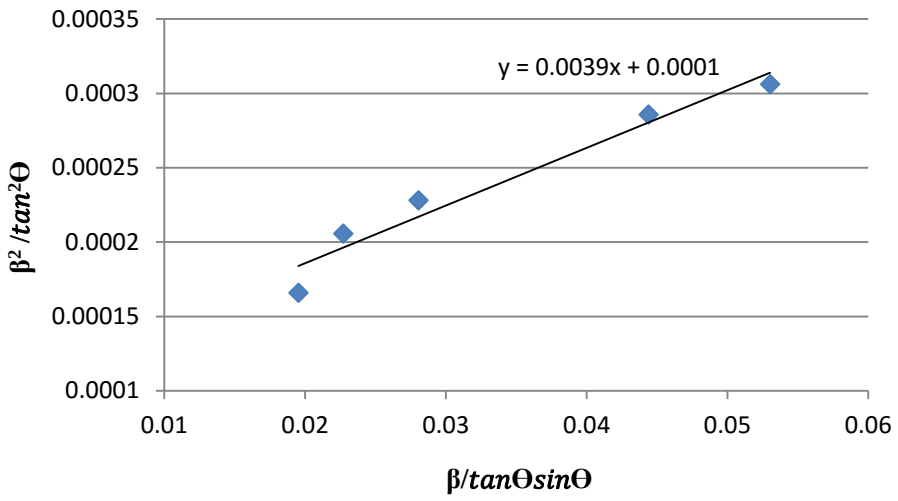

Figure 4. 2. Linear fit of the integral breadth analysis used to calculate the grain size and the lattice strain for as-milled Al-1%Sr

Al has been synthesized by mechanical milling by many researchers, and nano-grained structure had been attained. However in such reported literature, process control agents such as stearic acid and ethanol have been added to the Al powder inside the milling vial to prevent welding during milling [62], [107]–[110]. De Castro et al. [107] used ethanol in the milling process to produce 22 nm nc Al. Ammar et al. [108] used 5 wt% Stearic acid as a process control agent in the milling process and obtained nc Al with 18 nm grain size after milling for 6 hours. Abdoli et al. [110] used 1.5 wt% Stearic acid as a process control agent in the milling operation and obtained a 100 nm grain size after milling for 25 hours.

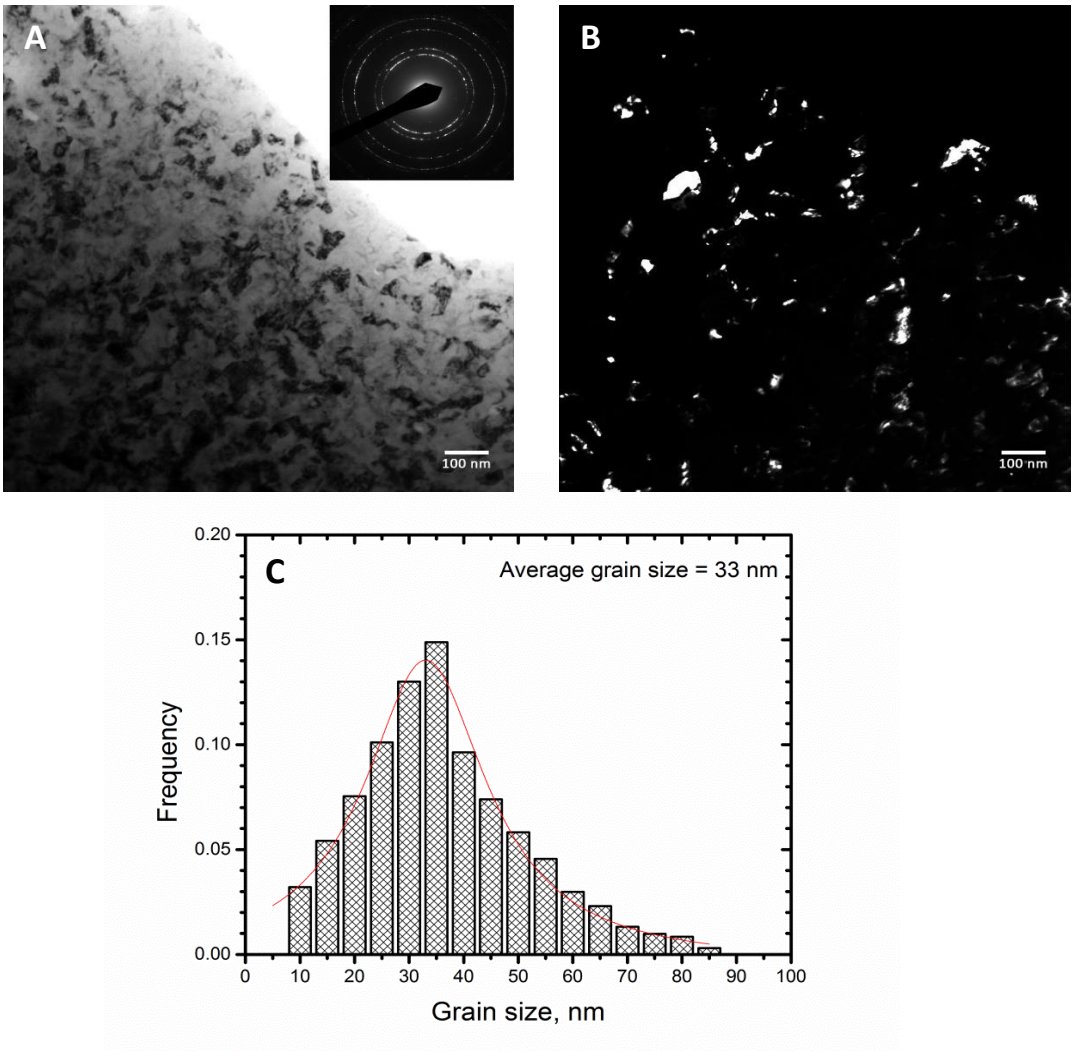

Figure 4. 3. Bright field (A), dark field (B) TEM micrographs, and grain size distribution of as milled nc Al, cryomilled for 6 hours (C)

Other researchers have synthesized nc Al by cryomilling with liquid nitrogen by adding nitrogen directly inside the milling vial [62], [111]. Zhou et al. [62] cryomilled Al by using 0.25 wt% stearic acid in addition to adding liquid nitrogen directly into the mill to assure complete immersion of the milling media and obtained nc Al of a grain size of 26

nm. Junsheng et al. [111] used a similar cryomilling technique to produce nc Al of a grain size of 42 nm after cryomilling for 12 hours.

In these cases, the nanometric grain sizes were attributed to the limiting of the recovery process during milling due to the cryogenic environment and contamination by AlN particles or to the introduction of oxygen and other impurity particles such Al_2O_3 from the process control agents [110], [112]. Hence grain structures were attained yet at the expense of the purity of their final product.

Mechanical properties of our as milled nc Al were investigated through Vickers microhardness tests and compared with the 0.2 GPa measured hardness of conventional grain size Al. As can be seen from Figure 4.4, the average microhardness of the as milled nc Al is 1.1±0.018 GPa. This hardness value is about six times higher than that of coarse grained Al.

In reports where process control agents or liquid nitrogen were used in the milling process of Al, high values of hardness were attained even after heat treatments such as sintering or annealing. In such cases, hardness values were attributed to the presence of impurity particles resulting from the use of process control agents or nitrogen in the milling process, in addition to the small grain size obtained from the milling process. Fuentes et all [113] used ethylene-bis-stearamide as a process control agent and produced a nc Al with a 30 nm grain size. They reported a 1.1 GPa Vickers microhardness of the mechanically milled Al powder.

In our cryomilling process, no process control agents were used. Rather liquid nitrogen was passed around the milling vial to prevent welding and recovery and at the same time preventing contamination by nitrogen. In this case, the high hardness of the mechanically milled Al can be attributed to the lattice strain and the large dislocation density introduced by the milling process, as well as the nano grain size of the Al powder.

4.2 Thermal Stability of Nanocrystalline Al

In order to investigate the thermal stability of nc Al, isothermal annealing was performed for one hour at 573 K, 673 K, 773 K, and 873 K. Figure 4.4 shows the variation of microhardness of nc Al as a function of annealing temperature. It can be seen that the hardness values decreased gradually with annealing temperatures from 1.1 GPa for the as milled nc Al, to 0.67 GPa at 573 K and 0.34 at 873 K.

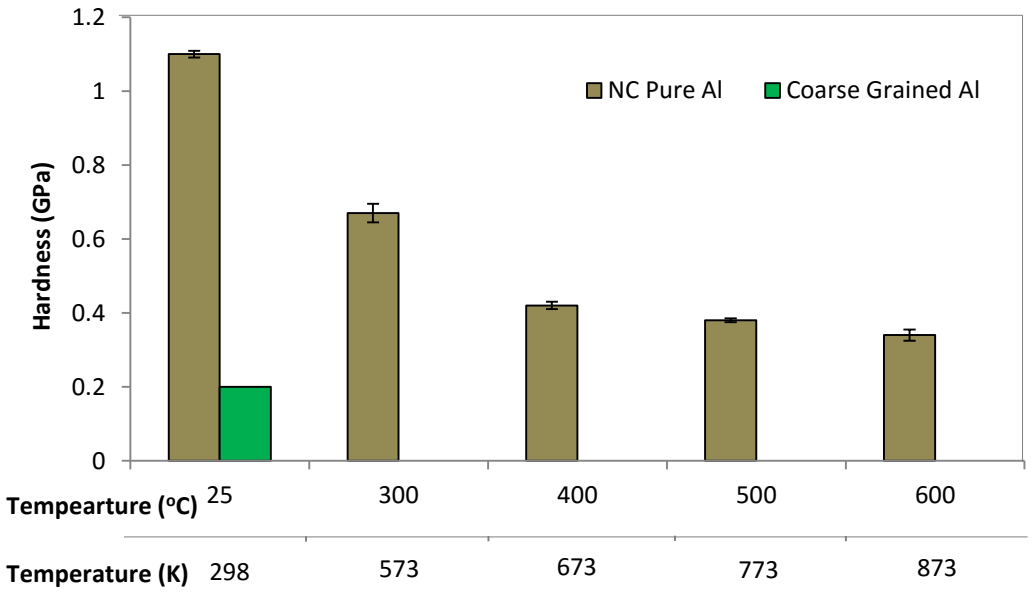

Figure 4. 4. Hardness vs. annealing temperature for nc Al and coarse-grained Al

The drop in hardness can be related to grain growth of the nc Al grains as the sample can no longer attain its ultrahigh hardness that originally generated as a result of grain

refinement. Figure 4.5 A and B show TEM micrographs for the nc Al samples annealed at 573 K and 873 K. Figure 4.5 C shows the grain size distribution for Al at 573 K. As can be concluded from the scale at both micrographs, the grains grew and the average grain size was measured to be 107±16 nm and 0.5-1 µm at 573 K and 873 K, respectively. The trend of thermal instability of nc Al with increasing temperature is in agreement with other results reported in literature [107]–[110], [113].

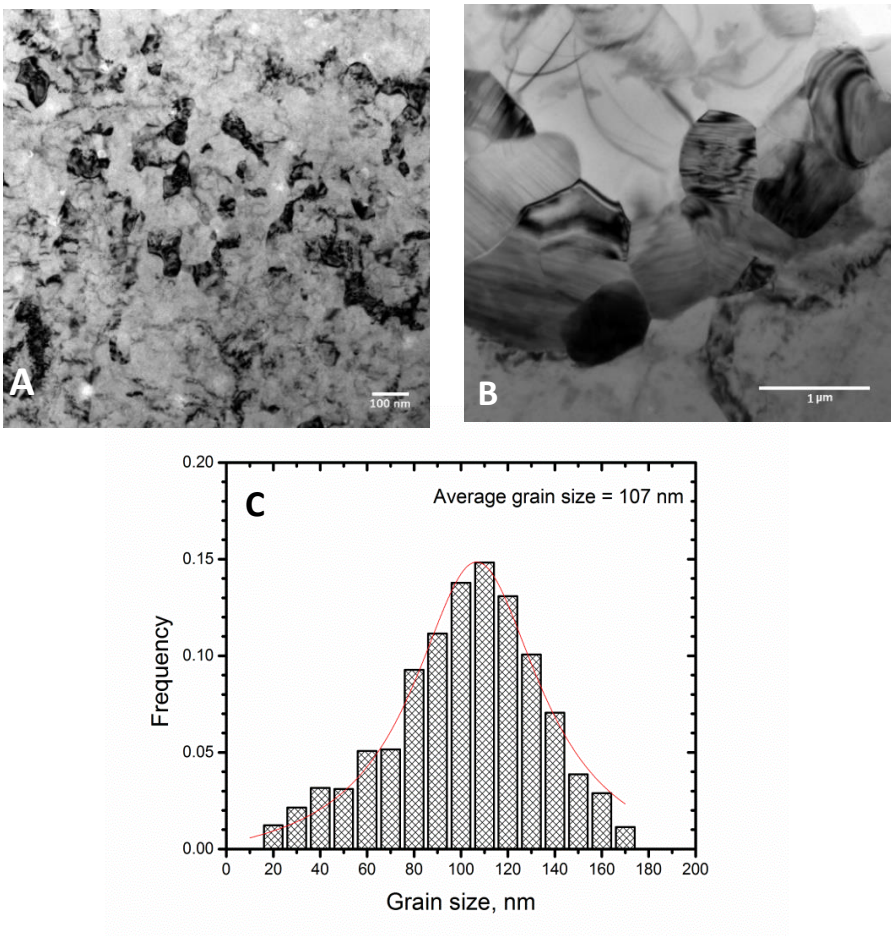

Figure 4. 5. Bright field TEM micrographs of nc Al annealed for one hour at 573 K (A) and 873 K (B). Grain size distribution of nc Al annealed for one hour at 573 K (C).

4.3 Effect of Adding 1at%Sr to Nanocrystalline As-Milled Al & Al-2 at.% Li

The effects of adding Sr on the thermal stability and hence the grain size and mechanical properties of nc Al and its Al-2 at.% Li alloy are discussed in this section.

4.3.1 Structural Analysis of As-Milled Samples

After synthesizing the samples by mechanical cryomilling for 6 hours, the microstructure of the as-milled Al-1 at.% Sr and Al-2 at.% Li-1 at.% Sr samples is studied through XRD analysis. Figure 4.6 show the XRD patterns for as milled Al-1 at.% Sr and Al-2 at.% Li-1 at.% Sr.

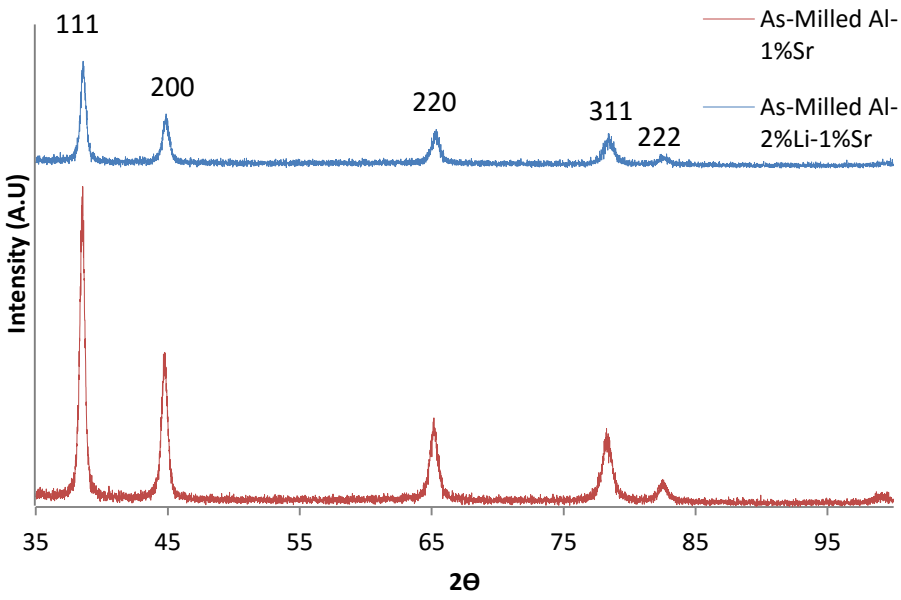

Figure 4. 6. XRD patterns for as-milled nc Al-1%Sr and Al-2%Li-1%Sr

Even after the addition of both 1 at.% Sr and 2 at.% Li, the positions of the peaks from the diffracted atomic planes indicated the presence of one FCC Al phase. According to the Al-Li phase diagram, the maximum solid solubility of Li in Al is between 3-4 at.% [114]. Hence, the absence of Li peaks in the diffraction pattern is simply due to the fact the 2 at.% Li completely dissolved into Al lattice to form a solid solution. However, looking at the phase diagram for Al-Sr shown in Figure 4.7, it is obvious that Sr has no solid solubility in Al, or in other words it is immiscible in Al, yet is absence in the as-milled peaks for Al-1 at.% Sr and Al-2 at.% Li- 1 at% Sr. This is accredited to the non-equilibrium synthesis process of mechanical alloying. It is reported that mechanical alloying can increase the solid solubility and lead to the formation of systems that otherwise are considered immiscible and would not form solid solutions in the conventional equilibrium state [61], [75]. Youssef et al. reported an increase in the maximum solid solubility of Mg in Al lattice from 1 wt.% to 4.5 wt.% after milling and in situ consolidation of Al-Mg [9].

Averbatch analysis were performed on all XRD peaks of both Al- 1 at.% Sr and Al-2 at.% Li-1 at.% Sr patterns shown in Figure 4.6. The grain size and strain calculated from the XRD line broadening using the Averbatch formula 25 nm and 0.2%, and 23 nm and 0.2%, for as milled nc Al-1 at.% Sr and as-milled nc Al-2 at.% Li-1 at.% Sr, respectively. It is obvious that the grain size of as milled nc Al, which was calculated to be 39 nm from the XRD pattern, is larger than that of the 25 nm grain size of Al-1 at.% Sr, even though both samples where synthesized under the same milling conditions. This is attributed to the fact that the addition of solute atoms such as Sr is reducing the ductility of Al and

making it more brittle by hindering the dislocation motion inside the Al lattice. Hence during the milling process, Al-1 at.% Sr is able to fracture easier than pure Al and overcome the welding of the grains in order to reach a small grain size.

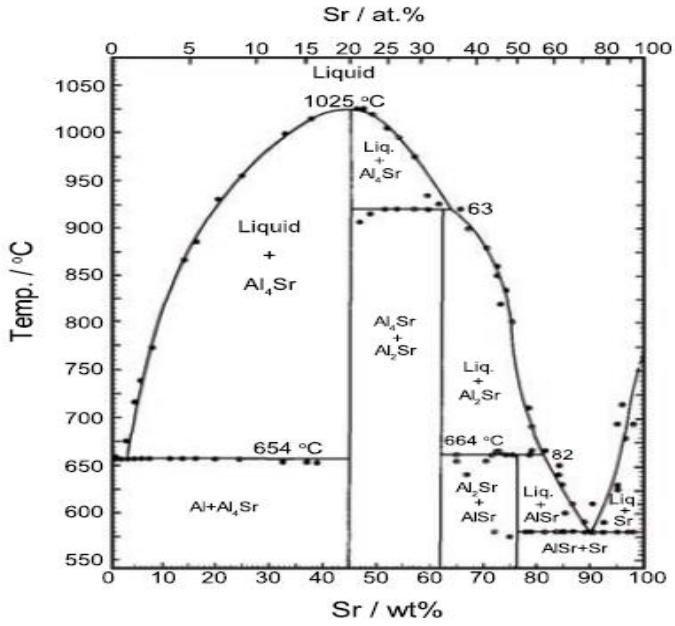

Figure 4. 7. Al-Sr phase diagram [116]

TEM analysis was conducted on as-milled Al-1 at.% Sr. Bright field and dark field TEM micrographs are shown in Figure 4.8 along with the grain size distribution, and the average grain size was measured to be 22±7 nm. Yet again, this grain size value measured by TEM is consistent with the 25 nm value calculated from the XRD pattern. This proves the accuracy of the XRD method for grain size calculations and gives the

confidence to use it as a reliable grain size calculating tool throughout the results of this thesis. At the end of the structural analysis section of the as-milled samples, we can conclude that cryomilling has successfully synthesized nc Al, Al-1 at.% Sr, and Al- 2 at.% Li- 1 at.% Sr.

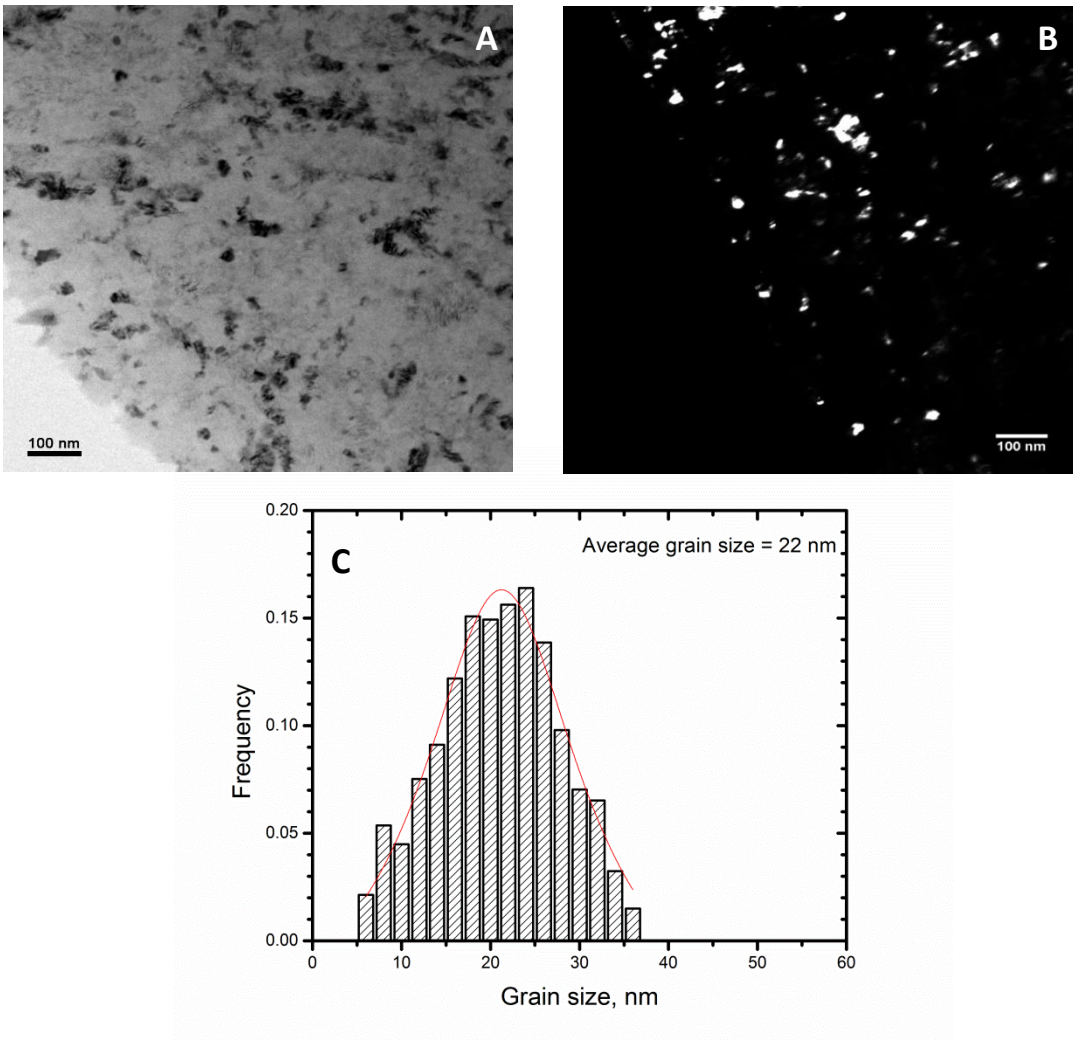

Figure 4. 8. Bright field (A), dark field (B) TEM micrographs, and grain size distribution of as milled nc Al-1%Sr (C)

4.3.2 Structural Analysis of Annealed Samples

Isothermal annealing of Al-1 at.% Sr and Al-2 at.% Li-1 at.% Sr was performed at different temperatures in order to examine their thermal stability. XRD was performed on the annealed Al-1 at.% Sr and Al-2 at.% Li-1 at.% Sr samples. Figure 4.9 shows the XRD patterns of the Al-1 at.% Sr as milled sample as well as the samples annealed at 673 K, 773 K, and 873 K. Two main points can be observed from Figure 4.9. The peaks of each pattern maintain their broadening even at higher annealing temperatures which is a result of grain size refinement and the introduction of lattice strain during the milling process. In addition, the peaks from the diffracted atomic planes suggest the presence of one dominant FCC Al phase over all ranges of annealing temperatures.

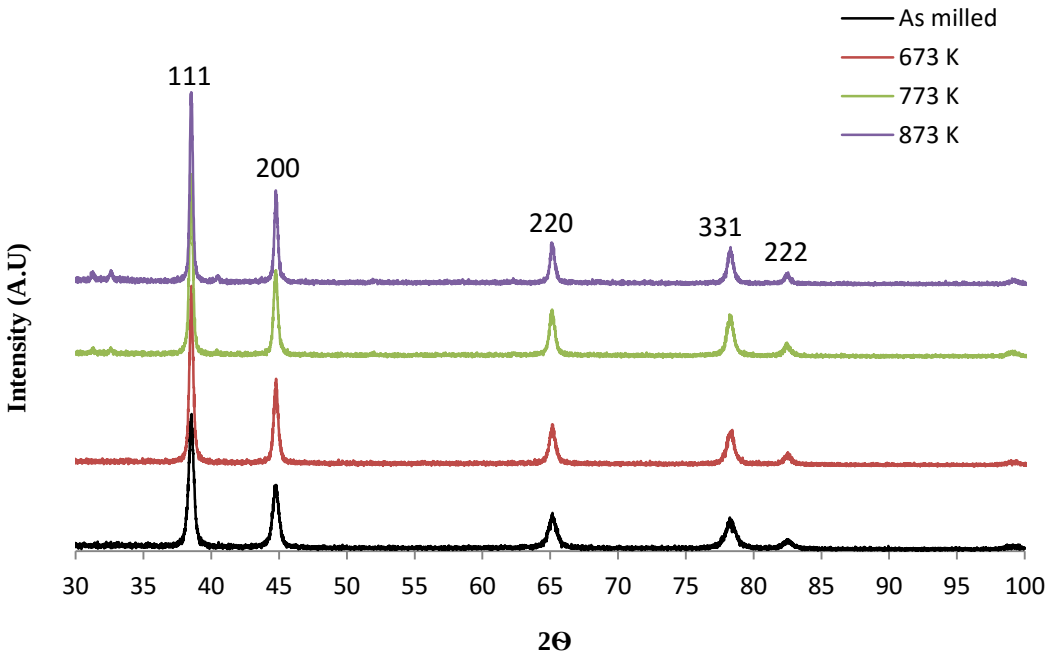

Figure 4. 9. X-ray diffraction pattern for as milled nc Al-1%Sr, 673 K, 773 K, and 873 K

The XRD line broadening was used to calculate the average grain size and lattice strain of the annealed Al-1 at.% Sr and Al-2 at.% Li-1 at.% Sr samples using the integral breadth analysis and the Averbatch formula. A least squares fit of the $\frac{(\beta)^2}{tan^2\theta_o}$ vs. $\left(\frac{\beta}{\tan\theta_o \sin\theta_o}\right)$ was obtained for all measured peaks of every sample. Figure 4.10 shows an example of that fit for the Al-1at%Sr sample annealed at 873 K. The 0.99 standard linear regression obtained indicates a good fit. The average grain size and the lattice strain obtained by the Averbatch method for both Al-1 at.% Sr and Al-2 at.% Li-1 at.% Sr are shown in Table 4.2.

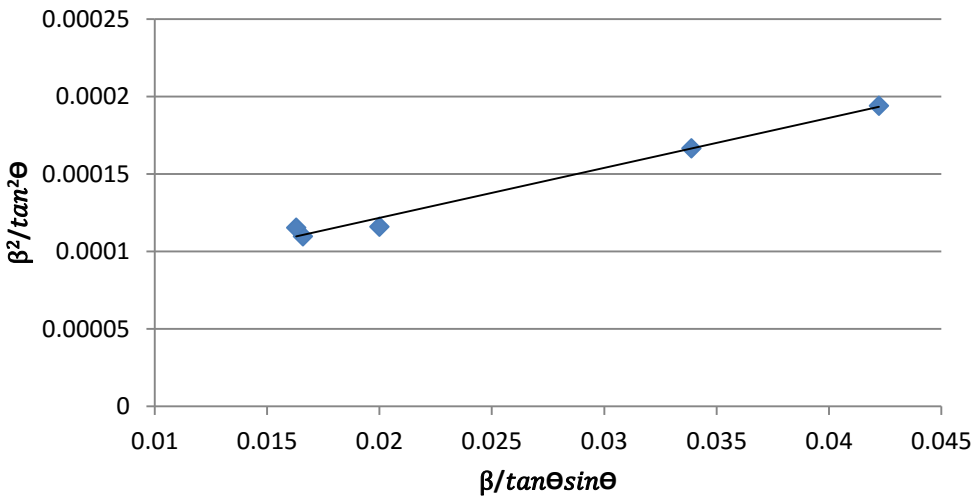

Figure 4. 10. An example of the linear fit of the integral breadth analysis used to calculate the grain size and the lattice strain for the Al-1%Sr sample annealed at 873 K

Table 4. 2. Grain size and lattice strain for both Al-1%Sr and Al-2%Li-1%Sr calculated by the Averbatch method

	NC Al-1 at.% Sr			NC Al-2 at.% Li-1 at.% Sr		
Temperature (K)	d (nm)	e (%)	R^2 (%)	d (nm)	e (%)	R^2 (%)
298 (as-milled)	25	0.2	94	23	0.2	90
573	-	-	-	32	0.19	98
673	37	0.19	96	-	-	
773	37	0.16	96	-	-	
873	48	0.15	99	61	0.17	98

It can be concluded that there is a drop in strain and a slight increase in grain size observed with increasing annealing temperature. This is consistent with the XRD pattern where the higher the temperature is, the sharper the peaks become. From Table 4.2, one can note that the grain size for both Al-1 at.% Sr at 673 K and 773 K is calculated to be 37 nm, where as they have different strain values. This is because heating can imposes two different effects on nanomaterials. It can lead to grain growth and it can reduce the strain in the material via dislocations annihilation [115]. Hence it seems that the second effect is observed in Al-1 at.% Sr at those temperatures.

Figures 4.11 and 4.12 show the TEM micrographs obtained for Al-1 at.% Sr annealed at 573 K and 873 K for one hour, respectively. In addition for annealing Al-1 at.% Sr at 873 K for 1 hour, A-1 at.% Sr was annealed at 873 K for a period of 24 hours to further investigate the stability of the sample at longer times of annealing.

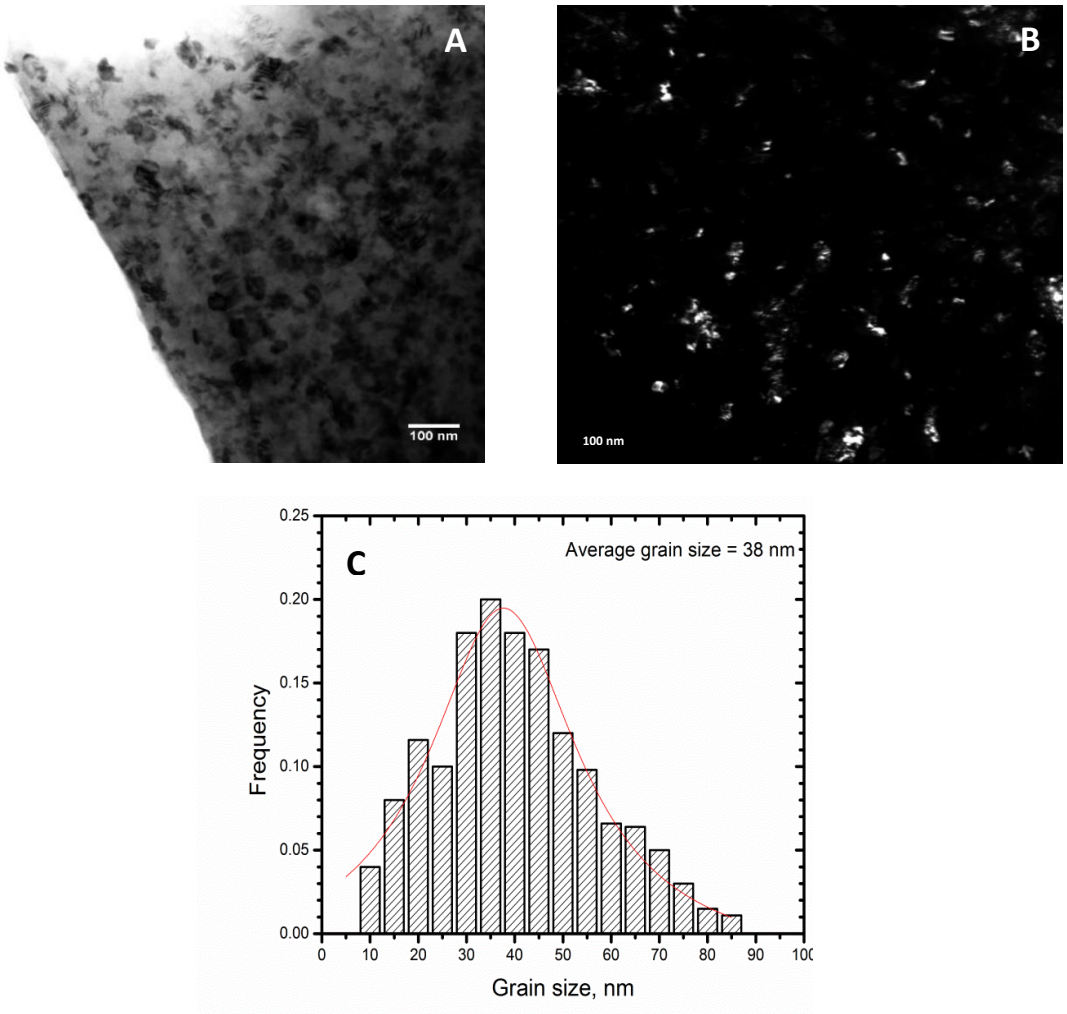

Figure 4. 11. Bright field (A), dark field (B) TEM micrographs, and grain size distribution (C) of nc Al-1%Sr annealed at 573 K.

As can be seen from Figures 4.11 and 4.12, grains in all micrographs are equiaxed with a monotonic distribution. The grain size as measured from Figures 4.11 A and 4.12 B are 38±13 nm and 50±12 nm for the samples annealed at 573 K and 873 K, respectively. Compared to the values reported in Table 4.2, these results confirm yet again the reliability of the grain size calculations from XRD.

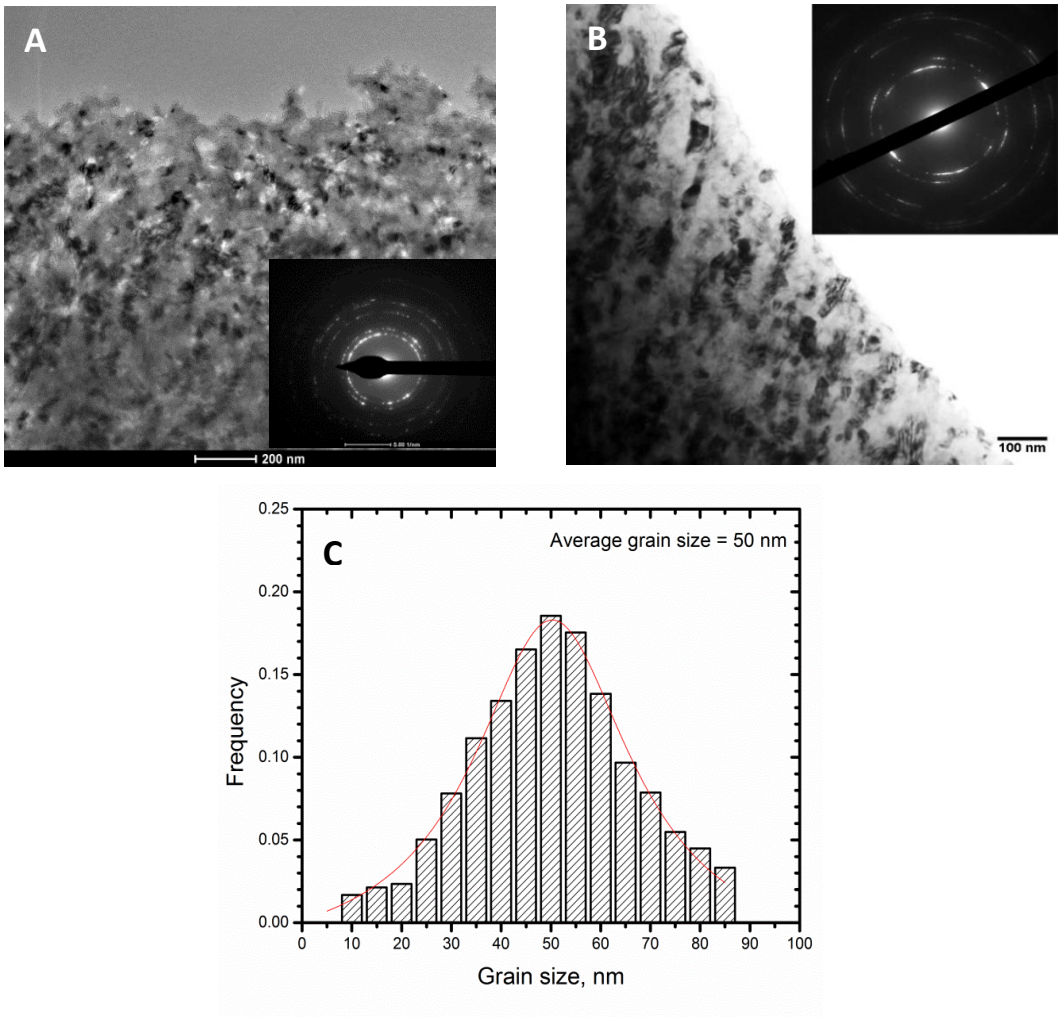

Figure 4. 12. Bright field TEM micrographs for Al-1%Sr annealed at 873 K for (A) 1 hour and (B) 24 hours. Grain size distribution for Al-1%Sr annealed at 873 K for 24 hours (C)

The grain size obtained from XRD calculations and TEM measurements vs. annealing temperature for Al-1 at.% Sr is shown in Figure 4.13. As can be seen, there is no significant difference between the grain size obtained by XRD or TEM. Figure 4.14 shows a comparison between the grain size of pure nc Al, nc Al-1 at.% Sr, and nc Al-2 at.% Li-1 at.% Sr as a function of annealing temperature. It is obvious that after the addition of Sr, grain size stability was maintained for nc Al and Al-2 at.% Li over the investigated temperature range.

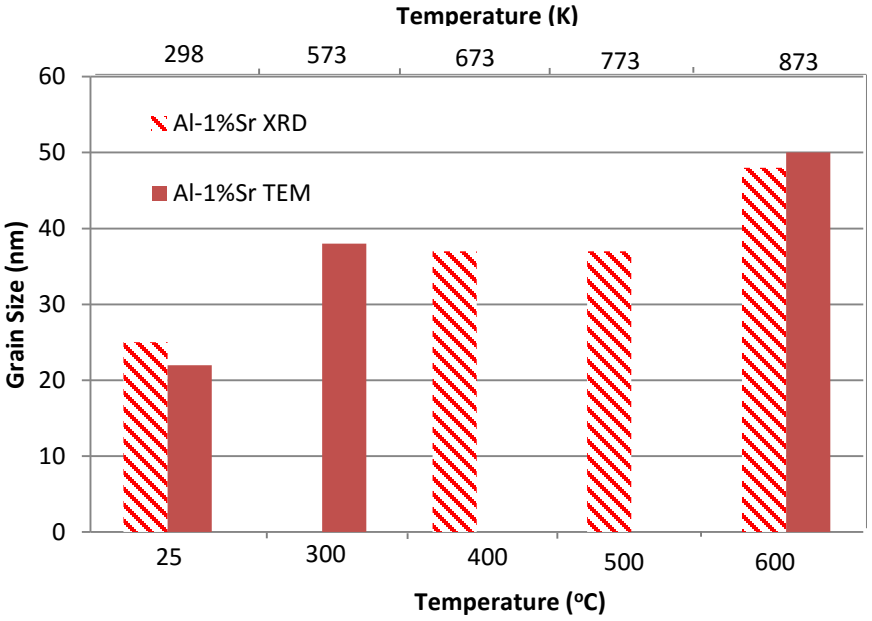

Figure 4. 13. Comparison of grain size obtained for Al-1%Sr from both XRD calculations and TEM measurements

The grain size of nc pure Al without Sr addition increased gradually with increasing temperature and approached a value of ~1 µm after annealing at 873 K. However, addition of 1 at.% Sr to Al and Al-2 at.% Li was able to stabilize the grain size within the nano range over the tested temperatures. As shown in Figure 4.14, the grain size values of Al-1 at.% Sr and Al-2 at.% Li-1 at.% Sr were 48 nm and 61 nm, respectively, after annealing at 873 K which represents 94% of its homologous temperature.

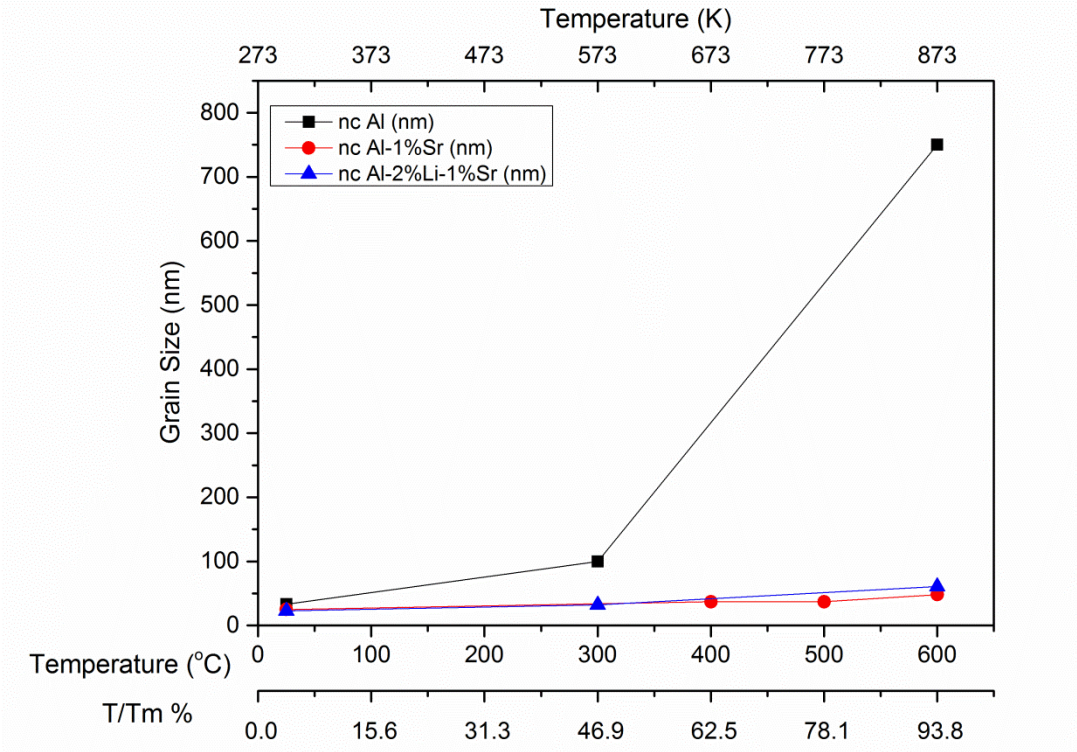

Figure 4. 14. Grain size vs. annealing temperature for nc Al, nc Al-1%Sr, and nc Al-2%Li-1%Sr

4.4. Thermal Stabilization Mechanism

Further information can be withdrawn from XRD patterns regarding the lattice structure of the Al-1 at.% Sr and Al-2 at.% Li-1 at.% Sr samples at different temperatures. This is of great importance as to identify whether the thermal stabilization of the nc metal is done kinetically by the introduction of a second phase or thermodynamically by lowering the Gibbs free energy of the system. In this discussion, we focus on the results obtained for Al-1 at.% Sr as the analysis of Al-2 at.% Li-1 at.% Sr results gave matching conclusions.

Referring back to Figure 4.9 which shows the XRD pattern for Al-1 at.% Sr, it was stated that the main peaks from the diffracted atomic planes indicated the presence of only one phase which corresponds to the Al FCC structure over the entire range of temperatures tested. Thus it can be concluded that Sr is dissolved into the crystal structure of FCC Al. Taking a closer look at the XRD pattern for Al-1 at.% Sr at 773 K and 873 K shown in Figure 4.9, new less intense peaks start to appear indicating the presence of a second phase. The new peaks occur at the same angles in both samples at 31.4, 32.7 and 40.4 degrees.

To investigate the new peaks, the Al-Sr phase diagram [116], shown earlier in Figure 4.7, was referred to. It can be seen that the first phase that can form after pure Al belongs to the intermetallic compound Al_4Sr. To further identify the new peaks, PCPDFWIN software was used in order to index those emerging peaks. Results confirmed that the new peaks belong to the Al_4Sr compound which has a tetragonal crystal structure, and

that the peaks belong to its three planes (103), (112), and (200). It is also clear from the XRD pattern for both samples, that the peaks become more intense at 873 K, this suggests that the formation and presence of this intermetallic compound increases with increasing temperature.

The presence of Al_4Sr intermetallic was also confirmed by Figure 4.15 which represents the TEM diffraction pattern obtained for Al-1 at.% Sr annealed at 873 K for 1 hour. It can be seen as indicated by the red arrows that in addition to the obvious Al FCC diffraction rings, new less intense rings are present at lower angles than (111) plane. This agrees with the XRD conclusion of the presence of an intermetallic second phase at high temperatures.

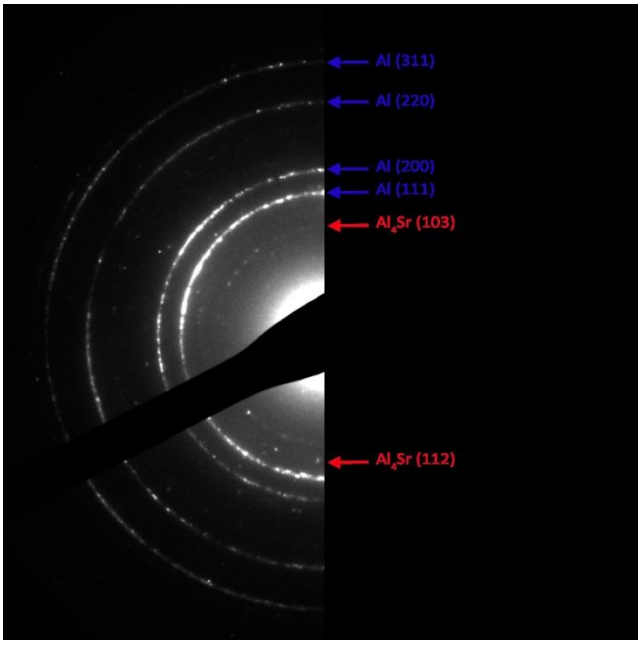

Figure 4. 15. TEM diffraction rings for Al-1%Sr annealed at 873 K for 1 hour

Lattice parameter calculations conducted using the Cohen method [97] were used to further investigate the new emerging peaks and the results are shown in Figure 4.16. The lattice parameter for pure as-milled Al was calculated to be 4.0492 Å, which is in agreement with the 4.05 Å value reported in literature [117]. Adding 1 at.% Sr to the as-milled sample increased the lattice parameter to 4.0528 Å. This is attributed to the addition of the large Sr atoms inside the Al FCC structure forming a solid solution, which is in agreement with the XRD patterns shown in Figure 4.9. However, the lattice parameter drops to 4.0516 and 4.0506 Å as the annealing temperature is increased to 773 K and 873 K, respectively. This is due to the fact that at these higher temperatures, Sr is able to diffuse out of the Al FCC lattice and form Al_4Sr intermetallic compound. This is in agreement with the Al-1 at.% Sr XRD pattern at 773 K and 873 K where the new Al_4Sr peaks started to emerge.

Youssef et al. [65] reported an increase in the lattice parameter of nc Cu from 3.616 Å to 3.627 Å as a result of mechanical alloying Cu with Nb. However, a gradual decrease in lattice parameter was recorded with increasing annealing temperatures. Authors attributed this behavior to the diffusion of the Nb atoms out of the Cu lattice to other lower energy sites in the grain boundaries. This trend of lattice parameter behavior is in agreement with the other results obtained for other systems [93], [118], [119].

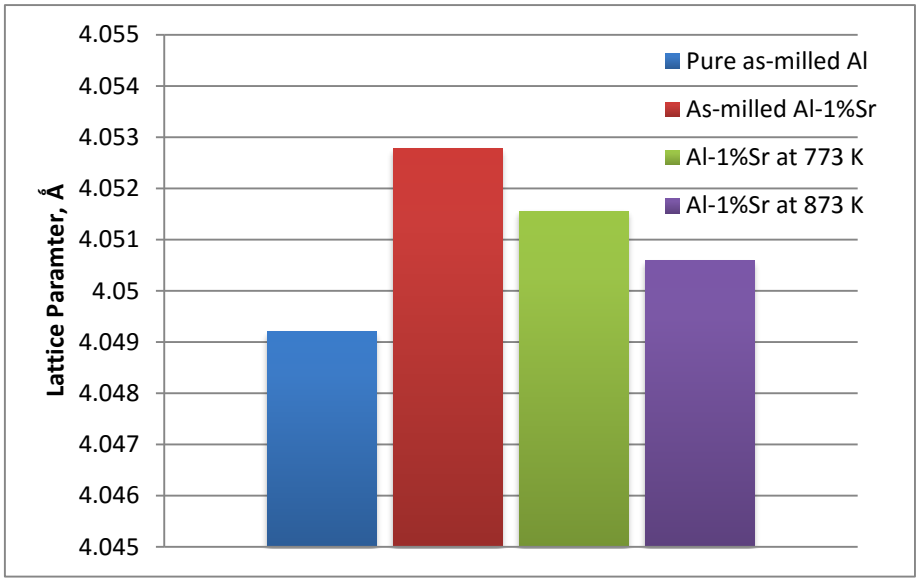

Figure 4. 16. Cohen method results for lattice parameter calculations of Al-1%Sr

The presence of the second phase Al_4Sr, even though only 1 at.% Sr is added to nc Al, can be attributed to the high temperatures at which the nc Al-1 at.% Sr sample was subjected to. In other words, at high temperatures, Sr gained enough energy to form an intermetallic compound. Most importantly, the presence of this second phase is believed to have contributed to the thermal stabilization of nc Al by the addition of 1 at.% Sr through second phase pinning at temperatures above 673 K.

According to the experimental results, we conclude that the thermal stabilization of nc Al up to 873 K or 94% of its homologous temperature is a two stage stabilization. The first is a thermodynamic one up to 673 K as there are no signs of second phases or precipitates up to this temperature. Hence Sr is able to thermodynamically stabilize the grain size of

nc Al by segregating to high energy regions in its grain boundaries, reducing its volume fraction, and reducing the overall free energy eliminating the need for grain growth.

The second stage however is accredited to the contribution of both thermodynamic and kinetic mechanisms at 773 K and 873 K. Even though the formation of the intermetallic second phase Al_4Sr is shown by XRD patterns and TEM which suggests the Zener drag mechanism contribution, the amount of Sr added is fairly low. Hence it is concluded that thermodynamic mechanism of Sr segregating to grain boundaries plays an important role as well at temperatures above 673 K, which helped in stabilizing nc Al grain size and hence its mechanical properties.

Darling et al. [120] reported the thermal stability of mechanically alloyed Fe by the addition of 4 at.% Zr where a 52 nm grain size was maintained to temperatures higher that 900 ^{o}C. At lower temperatures, the authors attributed the stabilization to the thermodynamic mechanism. However, once precipitation of intermetallic particles took place, the thermal stability was attributed to the combination of both thermodynamic and Zener pinning mechanisms at higher temperatures. These observations of a two stages thermal stabilization process, starting with thermodynamic before intermetallic phase formation, are in agreement with other several previously reported systems such as Fe-Cr [118].

Thermal stability of nc Al and Al alloys was investigated by several researchers [11], [62], [107], [108], [119]. Zhou et al. [62] studied the thermal stability and grain growth of a 26 nm nc Al which was synthesized by cryogenic mechanical milling through a series

of experimental procedures. A grain size of 50 nm was obtained up to 74% of the metal's homologous temperature. The thermal stability was attributed to solute drag rather than Zener pinning as authors suggested the volume fraction of the second phase precipitates such as aluminum oxide and aluminum carbide was too low for significant pinning of the grain boundary migration.

The thermal stability of $Al_{93}Fe_3Ti_2Cr_2$ alloy synthesized by mechanical alloying was studied by Shaw et al. [11]. The thermal stability was maintained up to 77% of the alloy's homologous temperature. The authors accredited the initial stability of the alloy to solute drag mechanism, however at higher temperatures than 450^{o}C, the formation of several second phases and intermetallic compounds starting with Al_6Fe and followed by Al_3Ti, $Al_{13}Fe_4$, and $Al_{13}Cr_2$, assured the contribution of Zener drag mechanism.

4.5 Mechanical Properties Measurements and Analysis

4.5.1 Hardness of Al-1 at.% Sr & Al-2 at.% Li-1 at.% Sr

A sign for thermal stability would be the ability for nc Al to maintain its exceptional mechanical properties at elevated temperatures, just as it maintained its grain size. Figure 4.17 shows the Vickers microhradness results for Al-1 at.% Sr and Al-2 at.% Li-1 at.% Sr, along with the microhardness results obtained for pure nc Al. With increasing annealing temperature, the hardness of pure nc Al decreases gradually and reaches a value of 0.34 GPa after annealing at 873 K for one hour. TEM analysis shows that the average grain size of pure Al increased to about 1 μm after annealing for 1 hour at 873 K, see Figure 4.5 A and B. The observed grain growth of nc Al is attributed to the high grain boundary energy of the 39 nm grain size that drives the grain growth process and accordingly decreases the hardness.

The role of Sr in the stability of nc Al and Al-2 at.% Li can be seen as exceptional hardness values of about 2.1 and 2.3 GPa obtained for the as milled Al-1 at.% Sr and Al-2 at.% Li-1 at.% Sr samples, respectively, compared to the hardness of 1.1 GPa for pure nc Al. This is attributed to the small grain size of the as-milled Al-1 at.% Sr (25 nm) and Al-2 at.% Li-1 at.% Sr (23 nm) compared to the grain size of as-milled Al (39 nm). In addition, solid solution strengthening resulted from the presence of the relatively large diameter Sr atoms into the Al lattice could also contribute to the high hardness values of Al-1 at.% Sr and Al-2 at.% Li-1 at.% Sr samples.

Furthermore, high hardness values of 1.2 and 1.6 GPa are still achieved upon annealing the Al-1 at.% Sr and Al-2 at.% Li-1 at.% Sr samples at 873 K. These values are even higher than that achieved by pure nc Al even at room temperature (1.1 GPa), and significantly much higher than that of 0.34 GPa obtained at 873 K. The significance of the high hardness values obtained at 873 K is due to the fact that this temperature is almost the melting temperature of Al and represents 94% of its homologous temperature. In addition to the nano grain size maintained for Al-1 at.% Sr and Al-2 at.% Li-1 at.% Sr at 600 ^{o}C of 48 nm and 61 nm, respectively, precipitation hardening which is a result of hindering the dislocation motion by the intermetallic Al_4Sr, plays a significant role in maintaining the high hardness values at higher temperatures.

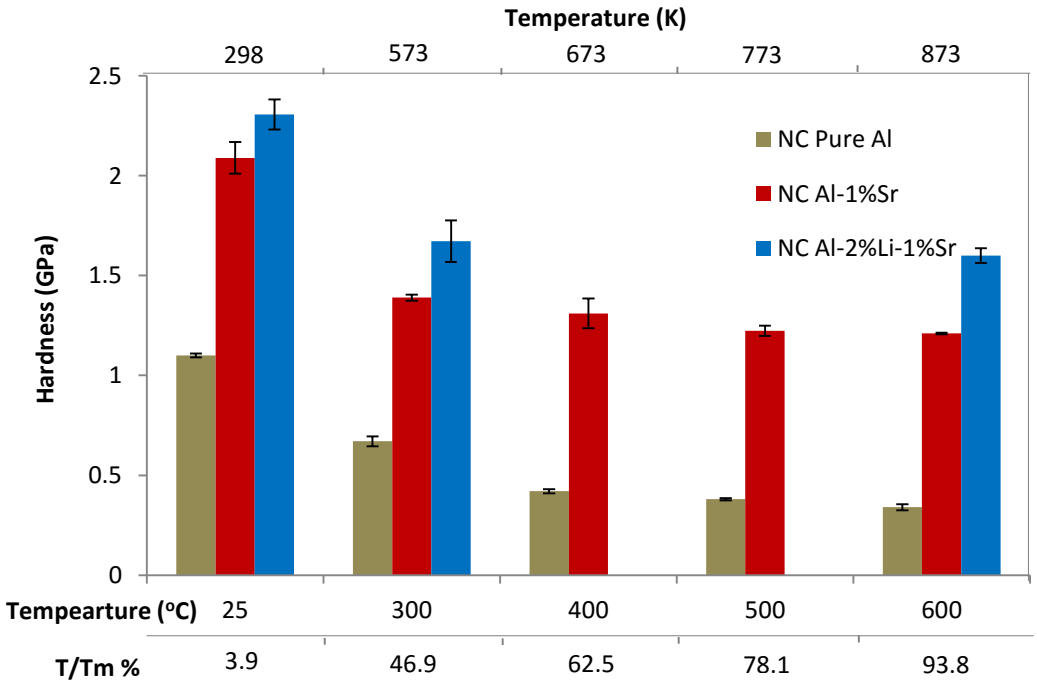

Figure 4. 17. Vickers microhardness vs. temperature of pure nc Al, nc AL-1%Sr and nc Al-2%Li-1%Sr

4.5.2 Ductility of Al-1 at.% Sr & Al-2 at.% Li-1 at.% Sr

One of the goals of this thesis is to produce thermally stable lightweight materials with high strength and good ductility. After achieving grain size and hardness stability of nc Al and Al-Li alloy through the addition of Sr, it is important at this stage to study the ductility of nc Al and its Al-Li alloy. As was mentioned in section 2, achieving high hardness and strength in nanomaterials had been in most of the cases at the expense of poor ductility [35]–[37], yet a few recent experimental studies reported the combination of exceptional strength with good ductility in nanomaterials [9], [14], [15], [23]–[25].

Shear punch test (SPT) allows for the characterization of the flow behavior of materials such as ductility in small samples. Hence, to test for ductility of Al-1 at.% Sr, SPT was conducted on different samples and followed by SEM to study the fracture surfaces of the tested samples. Figures 4.18 A and B show the shear stress vs. shear strain plots for Al-1 at.% Sr at 773 K and 873 K, respectively.

As can be noticed from the plots, two tests were done per condition, that is for Al-1 at.% Sr annealed at 773 K and 873 K, for reproducibility and the results are comparable indicating consistency in the material's mechanical response. From the behavior of the plots, it can be clearly concluded that the materials are undergoing plastic deformation, as the deformation continues well beyond the elastic region and maximum shear stress point. Average values of the maximum shear stress, uniform shear stress and maximum deformation obtained from Al-1 at.% Sr at 773 K and 873 K are listed in Table 4.3.

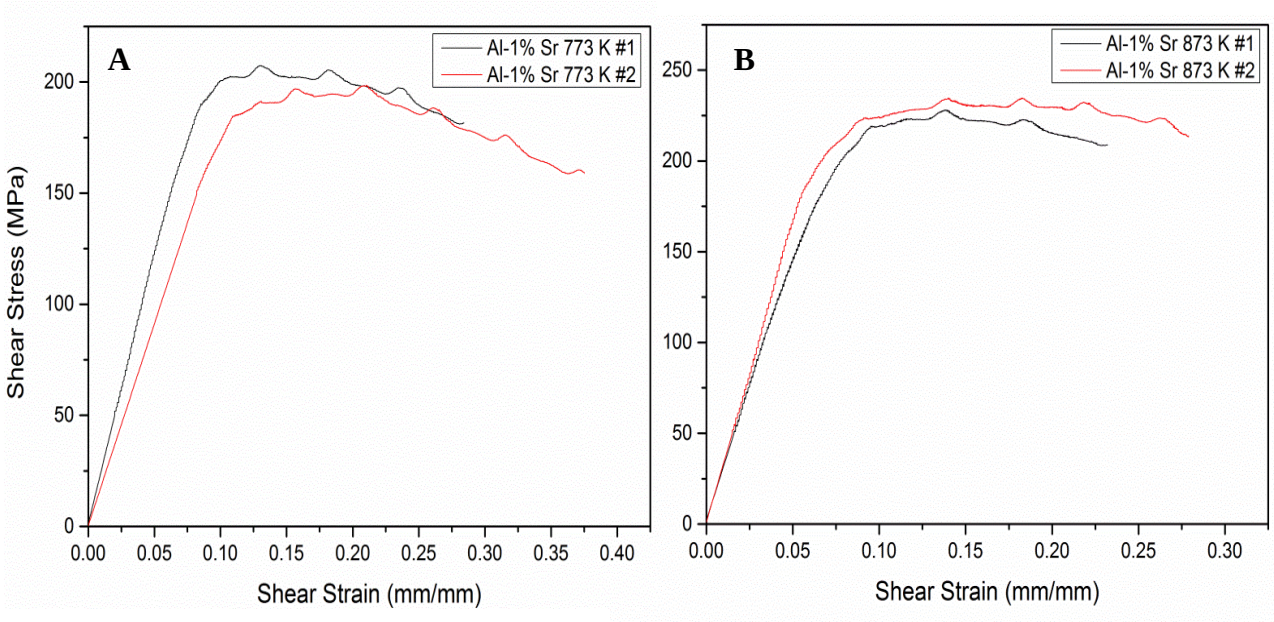

Figure 4. 18. Shear punch test stress vs. strain curves for Al-1%Sr annealed at 773 K (A) and 873 K (B)

Table 4. 3. Shear punch test results for Al-1%Sr at 773 and 873 K

	Al-1%Sr 773 K	Al-1%Sr 873 K
Maximum shear stress (MPa)	203 ± 4	231 ± 3
Uniform shear strain (mm/mm)	8% ± 0.03	6% ± $3x10^{-4}$
Maximum deformation (mm/mm)	25% ± 0.04	19% ± 0.03

It can be noticed from Table 4.3 that the maximum shear stress recorded for Al-1 at.% Sr at 873 K is 231 MPa and is larger than that of 202 MPa at 773 K. This can be justified by two reasons: enhanced density and precipitation hardening. We speculate that annealing the sample at 873 K resulted in a better consolidation and hence a higher density than that of the sample annealed at 773 K, as a result of the enhanced diffusion between the particles at higher temperatures. Hence, the Al-1 at.% Sr sample annealed at 873 K was able to withstand a higher maximum shear stress value as a result of its enhanced density. However, the more important justification is the precipitation hardening effect, which is also the reason for the higher maximum deformation percentage of 25% for Al-1 at.% Sr annealed at 773 K compared to that of 19% at 873 K. Referring back to Figure 4.9, it was shown that the formation of the intermetallic compound Al_4Sr starts at 773 K and increases at 873 K. Based on these results and observations, we may conclude that the higher strength and lower ductility of Al-1 at.% Sr annealed at 873 K is due to the presence of relatively high volume fraction of Al_4Sr which acts as an obstacle to the dislocation motion, the main mechanism responsible for ductility and plastic deformation.

SEM analysis of the fracture surface was conducted to further investigate the ductility results observed in the shear punch tests. Figure 4.19 show the SEM fracture surface for Al-1 at.% Sr at 773 K. The morphology of the fracture is different for ductile and brittle materials depending on their ability to undergo plastic deformation. Samples with little or no ductility exhibit smoother fracture morphology as little or no deformation occurs, and failure rather occur after crack initiation and propagation. Ductile materials however, exhibit a more irregular rough dimpled like morphology. This dimpled structure is a

result of void nucleation at grain boundaries and slip planes due to existing internal defects. These defects include dislocations created at grain boundaries, intergranular slip and grain boundary sliding. These voids grow and eventually become sites for nucleation of the observed dimples [121].

Figure 4.19 A shows SEM image of the punched disk, while B and C show a higher magnification of the fractured surface. From the morphology in C it is clear that this surface belongs to a ductile material, as the morphology resembles a dimpled structure which can be directly linked to higher ductility. Similar dimpled morphology has been observed for different nanostructured materials [122]–[124].

Good ductility in nc Al alloys had been reported previously [9], [39]. Youssef et al. [9] produced a 26 nm Al-5083 alloy by in-situ consolidation. The nano-alloy achieved a total elongation of 8.5% along with a 740 MPa ultimate tensile strength. Tellkamp et al. [39] synthesized another Al-5083 alloy that showed a similar good ductility of 8.4% elongation by cryomilling and HIP consolidation. However in this alloy the good ductility was achieved at the expense of a lower tensile strength of 462 MPa. The difference in the results of both studies is attributed to the difference synthesis techniques used to synthesize both alloys.

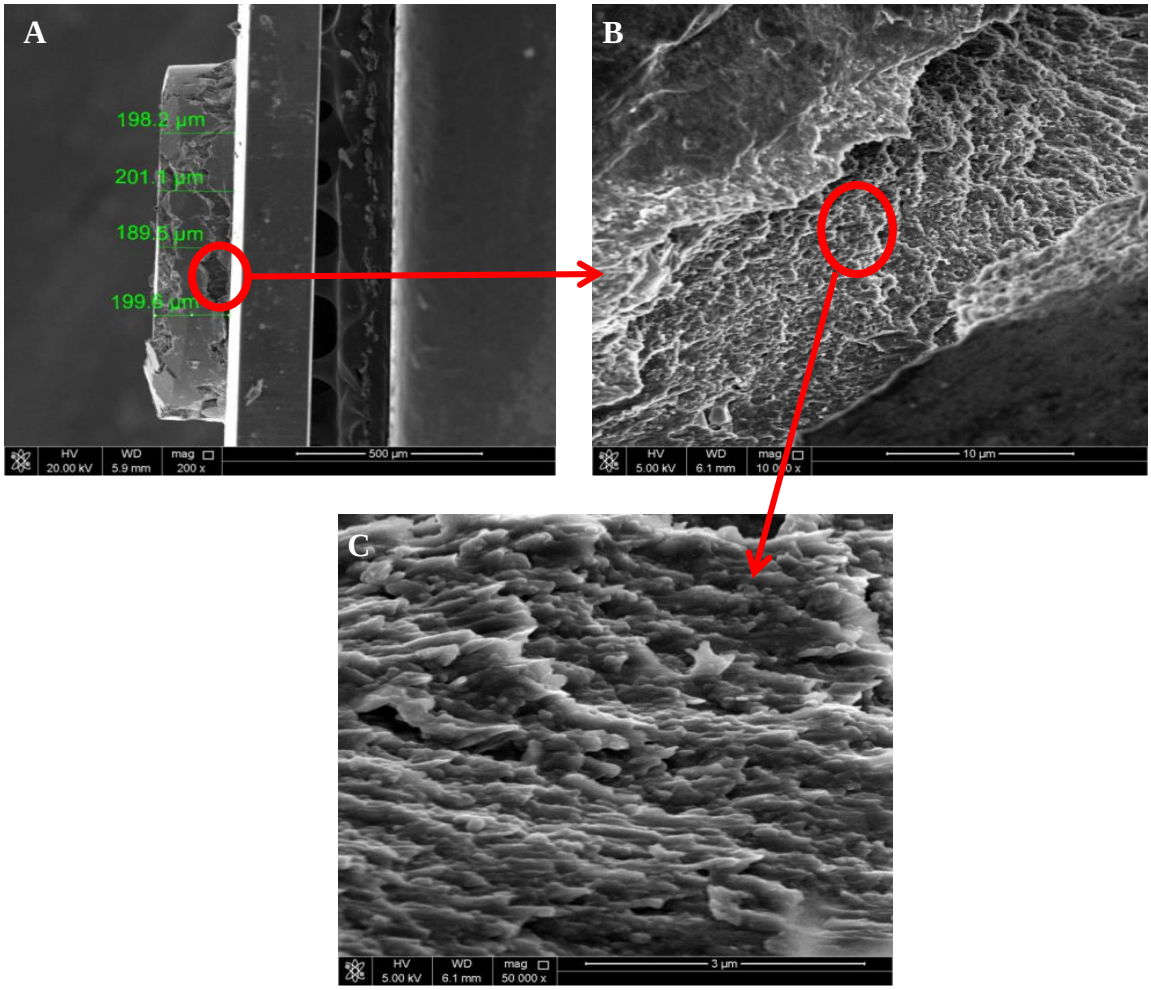

Figure 4. 19. SEM image of the Al-1%Sr shear punched disk annealed at 773 K (A), with increasing magnification to show the fracture surface morphology (B) and (C)

Chapter 5. Conclusion

The thermal stability and mechanical properties of nc Al and its light weight Al-Li alloy as a function of annealing temperature have been investigated. Mechanical milling of the powders was the synthesis process of choice with liquid nitrogen flowing around the vial to reduce the ductility of Al and prevent its welding.

Two mechanisms (thermodynamic and kinetic) have been developed to suppress grain growth in nanomaterials yet both of them depend on the addition of solute atoms. The first step towards achieving thermal stabilization is the selection of a suitable alloying element that will segregate to the grain boundaries and stabilize the grain size by reducing the driving force for grain growth. Based on our developed mathematical model, Sr was chosen as a suitable solute to suppress the growth in nc Al and Al-2 at.% Li alloy by the addition of just 1 at.% Sr.

The following are the conclusions established based on the results presented in this thesis:

1. The cryomilling technique was successfully utilized to synthesize nc Al with an average grain size value of 33nm.

2. The nc Al was found to be thermally unstable that its high hardness of 1.1 GPa decreased gradually with increasing annealing temperature and reached to 0.34 GPa at 873 K. The corresponding grain size of pure Al at that temperature was about 1 μm. This

suggested that the nanostructure attained by ball milling was lost when exposed to higher temperatures, which was proved by TEM studies.

3. Al-1 at.% Sr and Al-2 at.% Li-1 at.% Sr were successfully cryomilled to grain sizes of 25 nm and 23 nm, respectively. Addition of 1 at.% Sr led to thermal stabilization maintaining the grain size of nc Al (48 nm) and Al-2 at.% Li (61 nm) in the nano range up to 873 K.

4. High hardness values of 2.1 GPa and 2.3 GPa are obtained for the as milled nc Al-1 at.% Sr and Al-2 at.% Li-1 at.% Sr, respectively. Furthermore, high hardness values of 1.2 GPa and 1.6 GPa are still achieved upon annealing both samples at 873 K, which represents 94% of the samples homologues temperature.

5. Lattice parameter calculations from XRD results showed a relatively high value of 4.0528 Å at room temperature due to the large Sr atoms added to the FCC crystal structure of Al. However with increasing annealing temperature, the lattice parameter decreases. This is due to the fact that at these higher temperatures Sr was able to diffuse out of the Al FCC lattice and form Al_4Sr intermetallic compound.

6. According to the experimental results, two stage stabilization is suggested for the thermal stability of nc Al and Al-2 at.% Li through the addition of 1 at.% Sr up to 873 K or 94% of its homologous temperature. The first stage is a thermodynamic one, where up to 673 K it is believed that the Sr atoms segregate to the grain boundaries of Al and Al-Li and reduce the energy of the grain boundaries and hence the driving force for grain

growth. This conclusion is made based on the fact that no signs of second phases or precipitates were present up to this temperature. The second stage however is accredited to the contribution of both thermodynamic and kinetic mechanisms such as Zener pinning at 773 K and 873 K, due to the presence of the Al_4Sr intermetallic compound. These observations of a two stages thermal stabilization process, starting with thermodynamic before intermetallic phase formation, are in agreement with several previously reported systems.

7. Shear punch tests conducted on nc Al-1 at.% Sr suggests that the significant hardness obtained in this work was not at the expense of eliminating the ductility of Al as previous research suggested with other materials, and a 25% of maximum deformation was measured at 773 K. This was further proved by SEM studies which revealed the expected dimpled morphology of the fracture surface of ductile materials.

It is long overdue to design nc Al and Al-Li alloys for their best performance in the nanoscale. The combination of ultrahigh strength and improved ductility obtained in this thesis make what was impossible in the past possible today, such as producing superlight and ultra-tough nc Al-Li based alloys to be used in a variety of technological and structural applications.

Chapter 6. References

[1] K. Kumar, H. Van Swygenhoven, and S. Suresh, "Mechanical behavior of nanocrystalline metals and alloys," *Acta Mater.*, vol. 51, no. 19, pp. 5743–5774, 2003.

[2] M. A. Meyers, A. Mishra, and D. J. Benson, "Mechanical properties of nanocrystalline materials," *Prog. Mater. Sci.*, vol. 51, no. 4, pp. 427–556, 2006.

[3] O. Hall, E, "Variation of Hardness of Metals with Grain Size," *Nature*, vol. 173, p. 948, 1954.

[4] C. C. Koch, *Nanostructured Materials: Processing, Properties and Applications - Second Edition*. 2007.

[5] H. J. Fecht, E. Hellstern, Z. Fu, and W. L. Johnson, "Nanocrystalline metals prepared by high-energy ball milling," *Metall. Trans. A*, vol. 21, no. 9, pp. 2333–2337, 1990.

[6] C. Suryanarayana, "Nanocrystalline materials," *Int. Mater. Rev.*, vol. 40, no. 2, pp. 41–64, 1995.

[7] C. C. Koch, R. O. Scattergood, K. A. Darling, and J. E. Semones, "Stabilization of nanocrystalline grain sizes by solute additions," *J. Mater. Sci.*, vol. 43, no. 23–24, pp. 7264–7272, 2008.

[8] I. P. Polmear, "Light Alloys - From Traditional Alloys to Nanocrystals," *Light Alloy.*, vol. 2, pp. 273–277, 2006.

[9] K. M. Youssef, R. O. Scattergood, K. L. Murty, and C. C. Koch, "Nanocrystalline Al-Mg alloy with ultrahigh strength and good ductility," *Scr. Mater.*, vol. 54, no.

2, pp. 251–256, 2006.

[10] F. Zhou, J. Lee, and E. J. Lavernia, “Grain growth kinetics of a mechanically milled nanocrystalline Al,” *Scr. Mater.*, vol. 44, no. 8–9, pp. 2013–2017, 2001.

[11] L. Shaw, H. Luo, J. Villegas, and D. Miracle, “Thermal stability of nanostructured Al93Fe3Cr2Ti2 alloys prepared via mechanical alloying,” *Acta Mater.*, vol. 51, no. 9, pp. 2647–2663, 2003.

[12] C. E. Carlton and P. J. Ferreira, “What is behind the inverse Hall–Petch effect in nanocrystalline materials?,” *Acta Mater.*, vol. 55, no. 11, pp. 3749–3756, 2007.

[13] H. Gleiter, “Nanocrystalline Materials,” vol. 33, pp. 223–315, 1989.

[14] K. M. Youssef, Y. B. Wang, X. Z. Liao, S. N. Mathaudhu, L. J. Kecskés, Y. T. Zhu, and C. C. Koch, “High hardness in a nanocrystalline Mg97Y2Zn1 alloy,” *Mater. Sci. Eng. A*, vol. 528, no. 25–26, pp. 7494–7499, 2011.

[15] K. M. Youssef, R. O. Scattergood, K. L. Murty, J. A. Horton, and C. C. Koch, “Ultrahigh strength and high ductility of bulk nanocrystalline copper,” *Appl. Phys. Lett.*, vol. 87, no. 9, p. 091904, 2005.

[16] C. C. Koch, K. M. Youssef, R. O. Scattergood, and K. L. Murty, “Breakthroughs in optimization of mechanical properties of nanostructured metals and alloys,” *Adv. Eng. Mater.*, vol. 7, no. 9, pp. 787–794, 2005.

[17] H. Gleiter, “Materials with Ultra-Fine Grain Sizes,” in *2nd Risø International Symposium on Metals And Materials Science*, 1981, pp. 15–21.

[18] R. Siegel, “Synthesis and Processing of Nanostructured Materials,” in *Mechanical Properties and Deformation Behavior of Materials Having Ultra-Fine*

Microstructures, M. Nastasi, D. Parkin, and H. Gleiter, Eds. 1993, p. 509.

[19] G. Palumbo, S. Thrope, and K. Aust, "On the contribution of triple junctions to the structure and properties of nanocrystalline materials," *Scr. Metall. Mater.*, vol. 24, no. 7, pp. 1347–1350, 1990.

[20] H. Gleiter, "Nanostructured materials: basic concepts and microstructure," *Acta Mater.*, vol. 48, no. 1, pp. 1–29, 2000.

[21] J. R. Weertman, "Mechanical behavior of nanocrystalline metals," in *Nanostructured materials: processing, properties and potential applications*, C. Koch, Ed. Norwich (NY): Andrew Publishing, 2002, pp. 393–417.

[22] C. C. Koch, "Optimization of strength and ductility in nanocrystalline and ultrafine grained metals," *Scr. Mater.*, vol. 49, no. 7, pp. 657–662, 2003.

[23] K. Youssef, M. Sakaliyska, H. Bahmanpour, R. Scattergood, and C. Koch, "Effect of stacking fault energy on mechanical behavior of bulk nanocrystalline Cu and Cu alloys," *Acta Mater.*, vol. 59, pp. 5758–5764, 2011.

[24] S. Cheng, E. Ma, Y. M. Wang, L. J. Kecskes, K. M. Youssef, C. C. Koch, U. P. Trociewitz, and K. Han, "Tensile properties of in situ consolidated nanocrystalline Cu," *Acta Mater.*, vol. 53, no. 5, pp. 1521–1533, 2005.

[25] L. Lu, Y. Shen, X. Chen, L. Qian, and K. Lu, "Ultrahigh strength and high electrical conductivity in copper.," *Science*, vol. 304, no. 5669, pp. 422–426, 2004.

[26] G. D. Hughes, S. D. Smith, C. S. Pande, H. R. Johnson, and R. W. Armstrong, "Hall-petch strengthening for the microhardness of twelve nanometer grain diameter electrodeposited nickel," *Scr. Metall.*, vol. 20, no. 1, pp. 93–97, 1986.

[27] A. H. Chokshi, A. Rosen, J. Karch, and H. Gleiter, “ON THE VALIDITY OF THE HALL-PETCH RELATIONSHIP IN NANOCRYSTALLINE MATERIALS,” *Scr. Metall.*, vol. 23, pp. 1679–1684, 1989.

[28] X. Zhang, H. Wang, R. O. Scattergood, J. Narayan, and C. C. Koch, “Mechanical properties of cyromilled nanocrystalline Zn studied by the miniaturized disk bend test,” *Acta Mater.*, vol. 50, no. 13, pp. 3527–3533, 2002.

[29] Y. M. Wang, K. Wang, D. Pan, K. Lu, K. J. Hemker, and E. Ma, “Microsample tensile testing of nanocrystalline metals,” *Scr. Mater.*, vol. 80, no. 4, pp. 1017–1026, 2000.

[30] Y. Wang, M. Chen, F. Zhou, and E. Ma, “High tensile ductility in a nanostructured metal,” *Nature*, vol. 419, no. 6910, pp. 912–915, 2002.

[31] M. Legros, B. R. Elliott, M. N. Rittner, J. R. Weertman, and K. J. Hemker, “Microsample tensile testing of nanocrystalline metals,” *Philos. Mag. a-Physics Condens. Matter Struct. Defects Mech. Prop.*, vol. 80, no. 4, pp. 1017–1026, 2000.

[32] E. Botcharova, J. Freudenberger, and L. Schultz, “Mechanical and electrical properties of mechanically alloyed nanocrystalline Cu-Nb alloys,” *Acta Mater.*, vol. 54, no. 12, pp. 3333–3341, 2006.

[33] B. Han, F. Mohamed, and E. Lavernia, “Deformation Mechanisms and Ductility of Nanostructured Al Alloys,” in *MRS Proceedings*, 2004.

[34] T. T. Sasaki, T. Mukai, and K. Hono, “A high-strength bulk nanocrystalline Al-Fe alloy processed by mechanical alloying and spark plasma sintering,” *Scr. Mater.*, vol. 57, no. 3, pp. 189–192, 2007.

[35] C. Koch, D. Morris, K. Lu, and A. Inoue, “Ductility of nanostructured materials,” *MRS Bull.*, vol. 24, no. 2, pp. 54–58, 1999.

[36] J. R. Weertman, D. Farkas, K. Hemker, H. Kung, M. Mayo, R. Mitra, and H. Van Swygenhoven, “Structure and Mechanical Behavior of Bulk Nanocrystalline Materials,” *MRS Bull.*, vol. 24, no. February, pp. 44–53, 1999.

[37] C. C. Koch, “Ductility in Nanostructured and Ultra Fine-Grained Materials: Recent Evidence for Optimism,” *J. Metastable Nanocrystalline Mater.*, vol. 18, pp. 9–20, 2003.

[38] X. Zhang, H. Wang, R. O. Scattergood, J. Narayan, C. C. Koch, A. V. Sergueeva, and A. K. Mukherjee, “Studies of deformation mechanisms in ultra-fine-grained and nanostructured Zn,” *Acta Mater.*, vol. 50, no. 19, pp. 4823–4830, 2002.

[39] V. L. Tellkamp, E. J. Lavernia, and a. Melmed, “Mechanical behavior and microstructure of a thermally stable bulk nanostructured Al alloy,” *Metall. Mater. Trans. A*, vol. 32, no. 9, pp. 2335–2343, 2001.

[40] P. G. Sanders, C. J. Youngdahl, and J. R. Weertman, “The strength of nanocrystalline metals with and without flaws,” *Mater. Sci. Eng. A*, vol. 234–236, no. 1997, pp. 77–82, 1997.

[41] D. Jia, Y. M. Wang, K. T. Ramesh, E. Ma, Y. T. Zhu, and R. Z. Valiev, “Deformation behavior and plastic instabilities of ultrafine-grained titanium,” *Appl. Phys. Lett.*, vol. 79, no. 5, pp. 611–613, 2001.

[42] Y. M. Wang, E. Ma, and M. W. Chen, “Enhanced tensile ductility and toughness in nanostructured Cu,” *Appl. Phys. Lett.*, vol. 80, no. 13, pp. 2395–2397, 2002.

[43] C. Humphreys, “STEM Imaging of Crystals and Defects,” in *Introduction to Analytical Electron Microscopy*, 1st ed., J. Hern, J. Goldstein, and D. Joy, Eds. New York: Plenum Press, pp. 305–332.

[44] J. William, D. Callister, *Materials Science and Engineering: An Introduction*, 7th ed. Wiley & Sons, Inc., 2007.

[45] A. Cottrell, *Dislocation and Plastic Flow in Crystals*, 1st ed. Oxford University Press, 1953.

[46] R. Reed and H. R. Abbaschian, *Physical Metallurgy Principles*, 4th ed. Cengage Learning India, 2008.

[47] M. Dao, L. Lu, R. J. Asaro, J. T. M. De Hosson, and E. Ma, “Toward a quantitative understanding of mechanical behavior of nanocrystalline metals,” *Acta Mater.*, vol. 55, no. 12, pp. 4041–4065, 2007.

[48] G. W. Nieman, J. R. Weertman, and R. W. Siegel, “Mechanical behavior of nanocrystalline Cu and Pd,” *J. Mater. Res.*, vol. 6, no. 05, pp. 1012–1027, 1991.

[49] K. M. Youssef, R. O. Scattergood, K. L. Murty, and C. C. Koch, “Ultratough nanocrystalline copper with a narrow grain size distribution,” *Appl. Phys. Lett.*, vol. 85, no. 6, pp. 929–931, 2004.

[50] J. S. C. Jang and C. C. Koch, “The hall-petch relationship in nanocrystalline iron produced by ball milling,” *Scr. Metall. Mater.*, vol. 24, no. 8, pp. 1599–1604, 1990.

[51] J. A. Knapp and D. M. Follstaedt, “Hall-Petch relationship in pulsed-laser deposited nickel films,” *J. Mater. Res.*, vol. 19, no. 1, p. 218, 2004.

[52] C. Schuh, T. Nieh, and H. Iwasaki, “he effect of solid solution W additions on the mechanical properties of nanocrystalline Ni,” *Acta Mater.*, vol. 51, no. 2, pp. 431–434, 2003.

[53] A. Giga, Y. Kimoto, Y. Takigawa, and K. Higashi, “Demonstration of an inverse Hall-Petch relationship in electrodeposited nanocrystalline Ni-W alloys through tensile testing,” *Scr. Mater.*, vol. 55, no. 2, pp. 143–146, 2006.

[54] P. G. Sanders, J. a. Eastman, and J. R. Weertman, “Elastic and tensile behavior of nanocrystalline copper and palladium,” *Acta Mater.*, vol. 45, no. 10, pp. 4019–4025, 1997.

[55] C. S. Pande and K. P. Cooper, “Nanomechanics of Hall–Petch relationship in nanocrystalline materials,” *Prog. Mater. Sci.*, vol. 54, no. 6, pp. 689–706, 2009.

[56] D. J. Dunstan and A. J. Bushby, “Grain size dependence of the strength of metals: The Hall-Petch effect does not scale as the inverse square root of grain size,” *Int. J. Plast.*, vol. 53, pp. 56–65, 2014.

[57] R. Mitra, A. Chiou, and J. Weertman, “In Situ Study of Deformation Mechanisms in Sputtered Free-Standing Nanocrystalline Nickel Films,” *J. Mater. Res.*, vol. 19, no. 04, pp. 1029–1037, 2004.

[58] V. Yamakov, D. Wolf, S. R. Phillpot, A. K. Mukherjee, and H. Gleiter, “Dislocation processes in the deformation of nanocrystalline aluminium by molecular-dynamics simulation.,” *Nat. Mater.*, vol. 1, no. 1, pp. 45–48, 2002.

[59] J. Chen, L. Lu, and K. Lu, “Hardness and strain rate sensitivity of nanocrystalline Cu,” *Scr. Mater.*, vol. 54, no. 11, pp. 1913–1918, 2006.

[60] R. Valiev, “Ultrafine-Grained Materials Produced by Severe Plastic Deformation,” *Ann. Chim. Fr.*, vol. 21, pp. 369–378, 1996.

[61] C. Suryanarayana, “Mechanical alloying and milling,” *Prog. Mater. Sci.*, vol. 46, no. 1–2, pp. 1–184, 2001.

[62] F. Zhou, J. Lee, S. Dallek, and E. J. Lavernia, “High grain size stability of nanocrystalline Al prepared by mechanical attrition,” *J. Mater. Res.*, vol. 16, no. 12, pp. 3451–3458, 2001.

[63] F. Zhou, R. Rodriguez, and E. J. Lavernia, “Thermally stable nanocrystalline Al-Mg alloy powders produced by cryomilling,” *Metastable, Mech. Alloy. Nanocrystalline Mater.*, vol. 386–388, pp. 409–414, 2002.

[64] M. A. Atwater, R. O. Scattergood, and C. C. Koch, “The stabilization of nanocrystalline copper by zirconium,” *Mater. Sci. Eng. A*, vol. 559, pp. 250–256, 2013.

[65] K. M. Youssef, R. O. Scattergood, and C. C. Koch, “Remarkable Thermal Stability and Electrical Conductivity of Ultra-Tough Nanocrystalline Cu-1%Nb,” *Submitt. to Adv. Mater.*, 2014.

[66] M. A. Atwater, D. Roy, K. A. Darling, B. G. Butler, R. O. Scattergood, and C. C. Koch, “The thermal stability of nanocrystalline copper cryogenically milled with tungsten,” *Mater. Sci. Eng. A*, vol. 558, pp. 226–233, 2012.

[67] K. Boylan, D. Ostrander, U. Erb, G. Palumbo, and K. T. Aust, “An in-situ tem study of the thermal stability of nanocrystalline NiP,” *Scr. Metall. Mater.*, vol. 25, no. 12, pp. 2711–2716, Dec. 1991.

[68] K. a. a Darling, L. J. J. Kecskes, M. Atwater, J. Semones, R. O. O. Scattergood, and C. C. C. Koch, “Thermal stability of nanocrystalline nickel with yttrium additions,” *J. Mater. Res.*, vol. 28, no. 13, pp. 1813–1819, 2013.

[69] B. Huang, R. J. Perez, and E. J. Lavernia, “Grain growth of nanocrystalline Fe–Al alloys produced by cryomilling in liquid argon and nitrogen,” *Mater. Sci. Eng. A*, vol. 255, no. 1–2, pp. 124–132, 1998.

[70] H. Kotan, K. A. Darling, M. Saber, R. O. Scattergood, and C. C. Koch, “Thermal stability and mechanical properties of nanocrystalline Fe-Ni-Zr alloys prepared by mechanical alloying,” *J. Mater. Sci.*, vol. 48, no. 24, pp. 8402–8411, 2013.

[71] P. Cao, L. Lu, and M. O. Lai, “Grain growth and kinetics for nanocrystalline magnesium alloy produced by mechanical alloying,” *Mater. Res. Bull.*, vol. 36, no. 5–6, pp. 981–988, 2001.

[72] C. Kursun and M. Gogebakan, “Characterization of nanostructured Mg-Cu-Ni powders prepared by mechanical alloying,” *J. Alloys Compd.*, vol. 619, pp. 138–144, 2015.

[73] A. J. Detor and C. A. Schuh, “Tailoring and patterning the grain size of nanocrystalline alloys,” *Acta Mater.*, vol. 55, no. 1, pp. 371–379, 2007.

[74] K. Allen, “Thermal Stability of Nanocrystalline Microstructures,” North Carolina State University, 2009.

[75] P. C. Millett, R. P. Selvam, and A. Saxena, “Stabilizing nanocrystalline materials with dopants,” *Acta Mater.*, vol. 55, no. 7, pp. 2329–2336, 2007.

[76] J. R. Trelewicz and C. A. Schuh, “Grain boundary segregation and

thermodynamically stable binary nanocrystalline alloys," *Phys. Rev. B - Condens. Matter Mater. Phys.*, vol. 79, no. 9, pp. 1–13, 2009.

[77] L. C. Chen and F. Spaepen, "Analysis of calorimetric measurements of grain growth," *J. Appl. Phys.*, vol. 69, no. 2, pp. 679–688, 1991.

[78] K. A. Darling, "Thermal Stability of Nanocrystalline Microstructures," North Carolina State University, 2009.

[79] C. E. Krill, H. Ehrhardt, and R. Birringer, "Thermodynamic stabilization of nanocrystallinity," *Zeitschrift fuer Met. Res. Adv. Tech.*, vol. 96, no. 10, pp. 1134–1141, 2005.

[80] F. Liu and R. Kirchheim, "Comparison between kinetic and thermodynamic effects on grain growth," *Thin Solid Films*, vol. 466, no. 1–2, pp. 108–113, 2004.

[81] A. Michels, C. E. Krill, H. Ehrhardt, R. Birringer, and D. T. Wu, "Modelling the influence of grain-size-dependent solute drag on the kinetics of grain growth in nanocrystalline materials," *Acta Mater.*, vol. 47, no. 7, pp. 2143–2152, 1999.

[82] J. W. Cahn, "The impurity-drag effect in grain boundary motion," *Acta Metall.*, vol. 10, no. 9, pp. 789–798, 1962.

[83] M. Saber, "Thermal Stability of Nanocrystalline Alloys by Solute Additions and A Thermodynamic Modeling," North Carolina State University, 2013.

[84] B. K. VanLeeuwen, K. A. Darling, C. C. Koch, R. O. Scattergood, and B. G. Butler, "Thermal stability of nanocrystalline Pd81Zr19," *Acta Mater.*, vol. 58, no. 12, pp. 4292–4297, 2010.

[85] P. Knauth, A. Charaï, and P. Gas, "Grain growth of pure nickel and of a Ni-Si

solid solution studied by differential scanning calorimetry on nanometer-sized crystals," *Scr. Metall. Mater.*, vol. 28, no. 3, pp. 325–330, Feb. 1993.

[86] F. Humphreys and M. Hatherly, *Recrystallization and Related Annealing Phenomena*. Tarrytown: Elsevier Science, Inc., 1996.

[87] J. Weissmüller, "Alloy effects in nanostructures," *Nanostructured Mater.*, vol. 3, no. 1–6, pp. 261–272, 1993.

[88] R. W. Cahn and P. Haasen, "Physical Metallurgy," *North Holland Physics Publi.* Oxford, Amsterdam, p. 856, 1983.

[89] F. Liu and R. Kirchheim, "Grain boundary saturation and grain growth," *Scr. Mater.*, vol. 51, no. 6, pp. 521–525, 2004.

[90] T. Chookajorn, H. A. Murdoch, and C. A. Schuh, "Design of Stable Nanocrystalline Alloys," *Science (80-.).*, vol. 337, no. 6097, pp. 951–954, 2012.

[91] M. Saber, H. Kotan, C. C. Koch, and R. O. Scattergood, "A predictive model for thermodynamic stability of grain size in nanocrystalline ternary alloys," *J. Appl. Phys.*, vol. 114, no. 10, 2013.

[92] B. Farber, E. Cadel, A. Menand, G. Schmitz, and R. Kirchheim, "Phosphorus segregation in nanocrystalline Ni-3.6 at.% P alloy investigated with the tomographic atom probe (TAP)," *Acta Mater.*, vol. 48, no. 3, pp. 789–796, 2000.

[93] K. W. Liu, F. Mu, and F. Mücklich, "Thermal stability of nano-RuAl produced by mechanical alloying," *Acta Mater.*, vol. 49, no. 3, pp. 395–403, 2001.

[94] J. Weissmüller, W. Krauss, T. Haubold, R. Birringer, and H. Gleiter, "Atomic structure and thermal stability of nanostructured Y-Fe alloys," *Nanostructured*

Mater., vol. 1, no. 6, pp. 439–447, 1992.

[95] C. D. Terwilliger and Y. M. Chiang, "Size-dependent solute segregation and total solubility in ultrafine polycrystals: Ca in TiO2," *Acta Metall. Mater.*, vol. 43, no. 1, pp. 319–328, 1995.

[96] P. Wynblatt and D. Chatain, "Anisotropy of segregation at grain boundaries and surfaces," *Metallurgical and Materials Transactions A: Physical Metallurgy and Materials Science*, vol. 37, no. 9. pp. 2595–2620, 2006.

[97] B. D. Cullity, "Elements of X-ray diffraction, 2nd edition," *Addison-Wesley Publ. Co. Read. MA*, pp. 100–105,277–279, 1978.

[98] H. Klug and L. Alexander, *X-Ray Diffraction Procedures: For Polycrystalline and Amorphous Materials*. New York: John Wiley & Sons, 1974.

[99] M. U. Cohen, "Precision lattice constants from x-ray powder photographs," *Rev. Sci. Instrum.*, vol. 6, no. 3, pp. 68–74, 1935.

[100] D. B. Williams and C. B. Carter, *Transmission Electron Microscopy: A Textbook for Materials Science*, vol. V1–V4. 2009.

[101] D. V. S. Rao, K. Muraleedharan, and C. J. Humphreys, "TEM specimen preparation techniques," *Microsc. Sci. Technol. Appl. Educ.*, no. 320, pp. 1232–1244, 2010.

[102] A. E. Giannakopoulos, P. L. Larsson, and R. Vestergaard, "Analysis of Vickers indentation," *Int. J. Solids Struct.*, vol. 31, no. 19, pp. 2679–2708, 1994.

[103] D. Tabor, "The hardness and strength of metals," *J. Inst. Met.*, vol. 79, pp. 1–18, 1951.

[104] G. E. Lucas, J. W. Sheckherd, G. R. Odette, and S. Panchanadeeswaran, “Shear punch tests for mechanical property measurements in TEM disc-sized specimens,” *J. Nucl. Mater.*, vol. 122, no. 1–3, pp. 429–434, 1984.

[105] R. K. Guduru, K. A. Darling, R. Kishore, R. O. Scattergood, C. C. Koch, and K. L. Murty, “Evaluation of mechanical properties using shear-punch testing,” *Mater. Sci. Eng. A*, vol. 395, no. 1–2, pp. 307–314, 2005.

[106] J. Goldstein, D. Newbury, D. Joy, C. Lyman, P. Echlin, E. Lifshin, L. Sawyer, and J. Michael, *Scanning Electron Microscopy and X-ray Microanalysis*, vol. 1. 2003.

[107] C. L. De Castro and B. S. Mitchell, “Crystal growth kinetics of nanocrystalline aluminum prepared by mechanical attrition in nylon media,” *Mater. Sci. Eng. A*, vol. 396, no. 1–2, pp. 124–128, 2005.

[108] H. R. Ammar, K. A. Khalil, and E. M. Sherif, “Thermally Stable Nanocrystalline Aluminum Alloys Processed by Mechanical Alloying and High Frequency Induction Heat Sintering,” *Int. J. Chem. Mol. Nucl. Mater. Metall. Eng.*, vol. 9, no. 1, pp. 154–164, 2015.

[109] K. V. Rajulapati, R. O. Scattergood, K. L. Murty, G. Duscher, and C. C. Koch, “Effect of Pb on the mechanical properties of nanocrystalline Al,” *Scr. Mater.*, vol. 55, no. 2, pp. 155–158, 2006.

[110] H. Abdoli, M. Ghanbari, and S. Baghshahi, “Thermal stability of nanostructured aluminum powder synthesized by high-energy milling,” *Mater. Sci. Eng. A*, vol. 528, no. 22–23, pp. 6702–6707, 2011.

[111] C. Junsheng, C. Hua, C. Hanbin, Y. Bin, F. Jianzhong, and Z. Jishan, “Bulk

nanocrystalline Al prepared by cryomilling," *J. Univ. Sci. Technol. Beijing Miner. Metall. Mater. (Eng Ed)*, vol. 14, no. 6, pp. 523–528, 2007.

[112] L. Kurmanaeva, T. D. Topping, H. Wen, H. Sugahara, H. Yang, D. Zhang, J. M. Schoenung, and E. J. Lavernia, "Strengthening mechanisms and deformation behavior of cryomilled Al-Cu-Mg-Ag alloy," *J. Alloys Compd.*, vol. 632, pp. 591–603, 2015.

[113] J. J. Fuentes, J. A. Rodriguez, and E. J. Herrera, "Processing of mechanically alloyed aluminum powder: A metallographic study," *Mater. Charact.*, vol. 61, no. 4, pp. 386–395, 2010.

[114] F. W. Gayle, J. B. Vander Sande, and A. J. McAlister, "The Al-Li (Aluminum-Lithium) system," *Bull. Alloy Phase Diagrams*, vol. 5, no. 1, pp. 19–20, 1984.

[115] A. J. Detor and C. A. Schuh, "Microstructural evolution during the heat treatment of nanocrystalline alloys," *J. Mater. Res.*, vol. 22, no. 11, pp. 3233–3248, 2007.

[116] B. Closset, H. Dugas, M. Pekguleryuz, and J. E. Gruzleski, "The aluminum-strontium phase diagram," *Metall. Trans. A*, vol. 17, no. 7, pp. 1250–1253, 1986.

[117] W. P. Davey, "Precision measurements of the lattice constants of twelve common metals," *Phys. Rev.*, vol. 25, no. 6, pp. 753–761, 1925.

[118] M. Saber, H. Kotan, C. C. Koch, and R. O. Scattergood, "Thermal stability of nanocrystalline Fe-Cr alloys with Zr additions," *Mater. Sci. Eng. A*, vol. 556, pp. 664–670, 2012.

[119] M. Jafari, M. H. Enayati, M. H. Abbasi, and F. Karimzadeh, "Thermal stability and structural changes during heat treatment of nanostructured Al2024 alloy," *J.*

Alloys Compd., vol. 478, no. 1–2, pp. 260–264, 2009.

[120] K. A. Darling, B. K. VanLeeuwen, C. C. Koch, and R. O. Scattergood, "Thermal stability of nanocrystalline Fe-Zr alloys," *Mater. Sci. Eng. A*, vol. 527, no. 15, pp. 3572–3580, 2010.

[121] K. S. Kumar, S. Suresh, M. F. Chisholm, J. A. Horton, and P. Wang, "Deformation of electrodeposited nanocrystalline nickel," *Acta Mater.*, vol. 51, no. 2, pp. 387–405, 2003.

[122] H. Li and F. Ebrahimi, "Transition of deformation and fracture behaviors in nanostructured face-centered-cubic metals," *Appl. Phys. Lett.*, vol. 84, no. 21, pp. 4307–4309, 2004.

[123] R. A. Mirshams, C. H. Xiao, S. H. Whang, and W. M. Yin, "R-Curve characterization of the fracture toughness of nanocrystalline nickel thin sheets," vol. 315, pp. 21–27, 2001.

[124] C. Xiao, R. A. Mirshams, S. H. Whang, and W. M. Yin, "Tensile behavior and fracture in nickel and carbon doped nanocrystalline nickel," *Mater. Sci. Eng. A*, vol. 301, no. 1, pp. 35–43, 2001.